Engineering Geology 219 (2017) 74–91

Contents lists available at ScienceDirect

Engineering Geology

journal homepage: www.elsevier.com/locate/enggeo

A slope movement in a complex rock formation: Deformation measurements and DEM modelling

S. Assefa *, A. Graziani, A. Lembo-Fazio

Roma Tre University, Engineering Department, Civil Engineering Section, Rome, Italy

ARTICLE INFO

Article history:
Received 27 April 2016
Received in revised form 16 September 2016
Accepted 26 October 2016
Available online 29 October 2016

Keywords:
Marly-Arenaceous
Strength reduction
Distinct element modelling
Hydromechanical analysis

ABSTRACT

The case history of a deep-seated slope movement in a complex rock formation (Marly-Arenaceous Formation) is analyzed. The movement, monitored for more than 20 years, was recognized after the discovery of intense cracking in the concrete lining of a hydraulic tunnel running across the slope. The time history of displacements shows that the ongoing deformation process is essentially a stationary creep phenomenon, also influenced by transient variations in pore pressure distribution. The shearing zone is mainly formed by tectonized clay gouge and is characterized by a mobilized strength close to residual. The slope has been modelled (by DEM approach) as a complex blocky structure defined by several joint sets: bedding planes, inclined and sub-vertical joints. Different hypotheses about the geometry of the slip surface, compatible with field evidences, are discussed as well as their influence on the critical friction angle of the slope. The type of model adopted for rock mass, with continuous or staggered joints, influences the pre-failure deformation mode, but the failure conditions are not as much affected. Finally, the response of DEM models to the increase in water level at the toe of the slope and to the rise of the groundwater table inside the slope has been analyzed. The results of simplified models, without flow calculation, and coupled hydro-mechanical analyses are compared, finding some relevant differences.

© 2016 Elsevier B.V. All rights reserved.

1. Introduction

The slope movement analyzed in this study was recognized in 1985, after the excavation of a hydraulic tunnel in the right bank of the Chiascio River (Italy). The movement affects a large portion of a ridge which has the longitudinal direction approximately perpendicular to the river (Fig. 1). Just passed the sliding area, the river is crossed by a rockfill dam, which was intended to create a reservoir for water supply. The diversion tunnel, bored through a ridge on the right bank of the dam, has been operated only for a short period, in 1991–1992, not for regular water conveyance but only for a temporary deviation of the river flow during the construction of the bottom discharge of the dam.

The first evidence of an active slope deformation was the intense cracking of the concrete lining in a section of the diversion tunnel located well inside the ridge, at a distance from the intake of approximately 250 m, under an average overburden of 50 m. The damaged tunnel stretch was soon interpreted as the place where the tunnel axis intersects a deep-seated slip surface.

The entire area of the dam reservoir, included the sliding zone and the dam foundation, is formed by an outcrop of the Marly-Arenaceous Formation, a Miocene flysch characterized by alternating sequence of marl, sandstone and calcarenite layers. As observed in many flysch formations of Italian Apennines (Angelucci et al., 1967; Lembo-Fazio et al., 1990), joints are often slickensided as a consequence of tectonic shearing and bending deformation of strata.

The presence of major discontinuity planes of low strength represents a key factor for stability analysis in slope and dam engineering and has often required specific investigations (Oberti et al., 1986; Graziani et al., 2012). Weak layers of small thickness, such as clay interbeds or thin shear bands, may be easily overlooked during ordinary borehole investigations, particularly in structurally complex formations (D'Elia et al., 1998), such as flysch and layered limestone formations (Alonso et al., 1993; Hatzor and Levin, 1997; Graziani et al., 2009).

In the present case, it is likely that most of the sliding surface is seated along an over-thrust plane gently dipping towards the Chiascio River valley. This circumstance adds further complexity to the structural setting of the slope and can explain some particular features of the sliding mass, whose overall volume has been estimated of 18 Mm^3.

This study has been focused on the influence of rock mass structure (joint pattern, block shape) and pore pressure distribution on the mechanical response of the slope. First, the main results of the geotechnical investigations and displacements measurements performed in more than 20 years are discussed in order to obtain a reference framework for modelling. The kinematic characters of the movement are essentially those of a planar-sliding (average velocity of 13–17 mm/y) presumably localized along clay interbeds and tectonized gouge.

* Corresponding author.
E-mail address: sirajm2000@gmail.com (S. Assefa).

http://dx.doi.org/10.1016/j.enggeo.2016.10.014
0013-7952/© 2016 Elsevier B.V. All rights reserved.

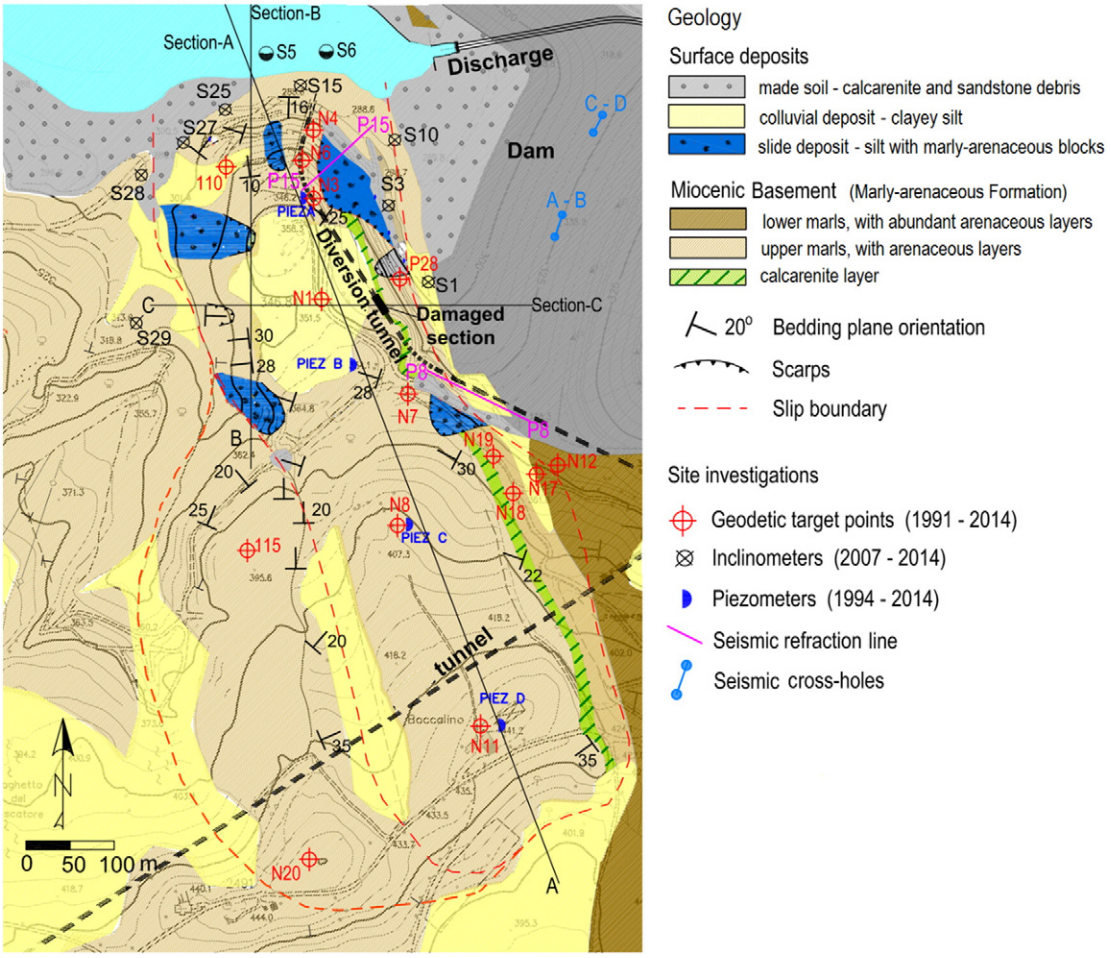

Fig. 1. Study area: geological setting, field investigation.

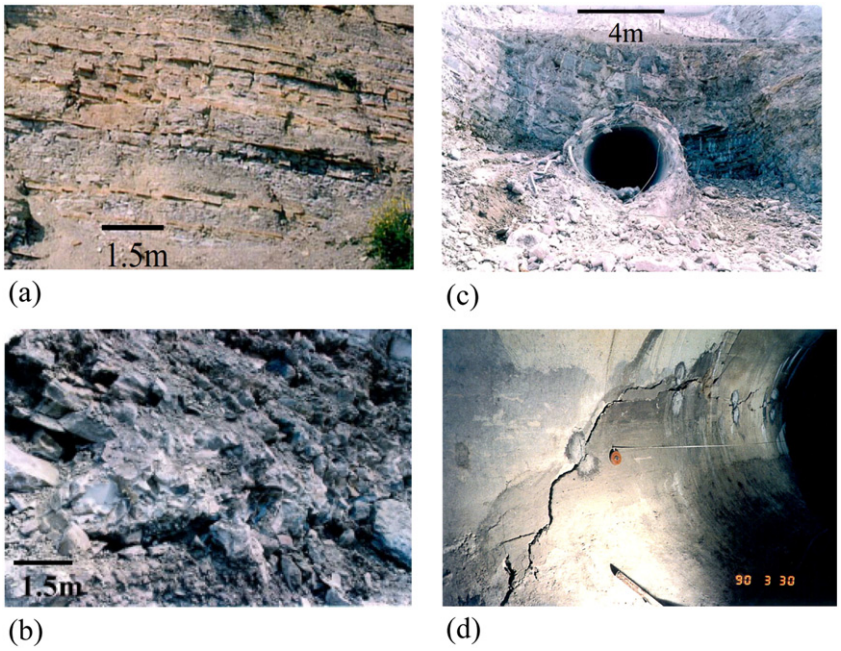

Fig. 2. Regularly layered rock mass in the East side of the ridge (a); disturbed rock mass at the toe of North slope (b); curved layers exposed during the excavation works for the diversion tunnel (c); main cracks and fissures seen in the concrete lining of the tunnel (d).

The structural setting of the slope has been modelled by a discontinuum medium approach (UDEC code, Itasca, 2011). Therefore, the influence of the rock mass structure (slip surface geometry, joint set orientation and continuity) on the deformation mode and the mobilized shear strength of the slope has been investigated. The pore pressure distribution inside the slope has been initially assigned by a water table, on the base of the average piezometric levels measured in four vertical boreholes. Then, coupled hydro-mechanical analyses have been also carried out, to analyze the influence of steady-state flow through the joint network for different reservoir levels.

2. Geological setting and morphology of the slope

The stretch of Chiascio River basin considered in this study is entirely based on a thick sequence of Miocene flysch deposits (Figs. 2 and 3). The main valley as well as the lateral gullies are carved in the same rock formation.

The Marly-Arenaceous Formation is characterized by a regularly layered structure, at least in its less disturbed portions (Celluzzi et al., 2014; Assefa et al., 2014). The different stratigraphic units can be distinguished essentially on the base of the lithology prevailing in the rock layers:

a) Lower marls unit, with rare thin layers of clay shale,
b) Mixed Marly-Arenaceous-calcarenitic unit,
c) Calcarenite unit, sparsely present as single layers,
d) Upper marls unit.

The lower marls are characterized by a more regular and continuous bedding. The a) unit was mostly exposed during the excavation for dam foundation, nearby the toe part of the sliding area (Fig. 1). The excavation works, started in 1984, required the removal of alluvium, debris and loosened rock up to 15 m depth below the river bed elevation.

The slope movement affects a large portion of a long ridge, upstream to the right abutment of the dam. The sliding mass is mostly composed of alternating layers (thickness, 0.1–0.2 m) of unit b) lithotypes, with the upper marls unit and shallow debris deposits at the top. The Calcarenite unit consists of two separate strata (each one formed by single layers of 0.1–1 m for a total thickness of 3–4 m) intermingled with the thinner layers of unit b).

While the upper portion of the ridge is gently dipping (10°) towards the Chiascio valley, the N side slope and the lateral flanks are steep (25–40°) and mostly covered by a talus of rock debris in a matrix of remolded clay. This situation hampers the visual detection of any trace of the slip surface at the toe of the slope (located at el. 270 m a.s.l., approximately). The upper limit of the ridge (S sector) is characterized by a plateau, located at an average elevation of 395 m a.s.l.

In the east flank of the ridge a regular monocline structure (bedding planes dipping to W, dip angles of 20–40°) can be clearly identified. The same structure, with remarkably continuous and consistent orientations of the bedding joints, was observed also on the foundation surface of the dam, as recorded in the construction reports. Conversely, the W flank of the ridge (bordered by a gully called "Fosso della Torre") is characterized by a less consistent orientation of bedding, especially in the lower part, where the orientation is more dispersed, although dip directions from E to NE seem prevailing, with dip angle of 25–50°. Therefore, the overall set up of the bedding planes suggests the hypothesis of a syncline structure, with axial plane having approximately N-S direction.

The N sector of the ridge could be carefully inspected during the excavation works for the intake structure of the diversion tunnel (Fig. 2c) and, after the discovery of the movement, by extensive borehole investigations. In this area the rock mass exhibits a high degree of fracturing and disarrangement of the bedded rock.

A fundamental evidence acquired from borehole loggings for the N sector is the presence of quaternary alluvium under the Miocene flysch forming the toe of the slope (Fig. 3). This circumstance can be reasonably explained as the consequence of an ancient overthrust deformation. By comparing the position of the contact between alluvium and Marly-Arenaceous formation in the different boreholes, it can be argued that the basal plane of the overthrust is almost horizontal and is located at an elevation slightly lower than the river bed (Assefa et al., 2015). The cumulated amount of horizontal displacement in the overthrust deformation coulb be as high as 100–150 m. If such hypothesis holds true, it is likely that also the current deformation process mostly occurs along the same shear band, i.e., through a layer of strongly tectonized clay gouge, at least for the lower portion of slip surface.

3. Survey of tunnel damage and slope displacement

As already mentioned, the occurrence of a slow movement in the ridge crossed by the diversion tunnel was recognized only after the completion of the tunnel lining. Nowadays, surface evidences of the ongoing deformation can also be detected, especially on the E boundary of the sliding area, where the pavement and curbs of some country roads appear locally displaced and fissured.

The diversion tunnel departs from the right flank of the valley, at an elevation of 286 m a.s.l., approximately 15 m higher than the toe of the slope, and runs through the long ridge with a direction almost perpendicular to the river (Fig. 1) for some 900 m, before turning to the W, taking a N238° direction.

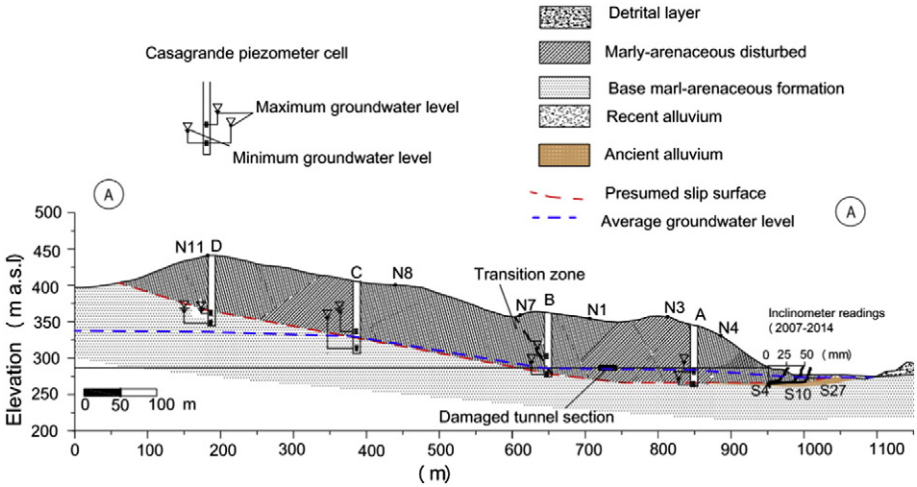

Fig. 3. Longitudinal cross-section of the moving ridge with relevant geological data, location of piezometer boreholes A, B, C and D, position of some geodetic targets (N1 … N11).

The first evidence of an active deep-seated movement came from the heavy damage of the tunnel lining, not yet in operation, which consists of a 4.5 m diameter, 0.5 m thick cast concrete ring. Cracking and opening of the construction joints were localized in a 23 m long stretch of tunnel, between chainage 235 and 258 m from the intake section. The limited width of the damaged stretch is strongly suggestive of a deep movement characterized by localized shearing. The damaged section of the tunnel is under an average overburden of 50 m and is located, in plan, some 40 m inside the lateral boundary of the movement.

The fissures in the lining were repeatedly sealed but formed again, then four 4 couples of crack-meters were installed across the main fissures (Fig. 2d). A clear picture of the relative displacement trend was obtained in 1991–1992, during a short period of operation of the diversion tunnel as temporary discharge in order to allow the completion works of the dam bottom outlet. In that period, the reservoir water level reached the maximum elevation of 296.5 m. After 3 months of tunnel operation, with average water level at 287 m a.s.l., the maximum allowable stroke (50 mm) of the displacement gauges was achieved. The relative displacement vectors measured across the cracks exhibited a negligible plunge and a direction close to the tunnel axis.

3.1. Geodetic survey of displacements

A first network of targets (N1–N11) for the geodetic survey of surface displacements, restricted to the frontal slope of the ridge (N sector), was implemented to integrate the crack-meters installed in the damaged section of the tunnel, before starting the temporary filling of the dam pool. The geodetic network was thereafter extended to the S and W areas, with targets (N12–N20) installed at greater distances from the N slope, in order to estimate areal distribution and limits of the movement (Fig. 1).

Since then, all the targets have been continuously monitored by a total station, installed on the opposite side of the valley, at the top of the concrete walls of the dam spillway. Measurements are performed regularly once a month. The prevailing components of displacement are those in the horizontal plane; the vertical component is much smaller and usually is not processed.

3.2. Tunnel extensometer

In 1994, it was decided to install a steel lining within the damaged section of the tunnel. This lining is formed by two coaxial pipes; the annular gap between the two steel pipes was not sealed but endowed with a "telescopic joint", in order to accommodate differential axial displacements between the two tunnel stretches separated by the cracked zone and, therefore, located, respectively, inside and outside the sliding portion of the rock mass. The telescopic joint was supplemented by an electric dial gauge, thereafter referred to as "tunnel extensometer".

3.3. Inclinometer measurements

The displacement data available after some years of geodetic survey were instrumental to trace the approximate boundaries of the sliding area. The lateral limit of the movement along the E flank of ridge were considered with particular attention due to proximity of the right abutment of the dam. Therefore, it was decided to refine the survey by installing a set of inclinometer tubes (Fig. 1). To take advantage of the shallow depth of the slip surface in the peripheral zone of the movement, the inclinometers have been installed mostly at the toe of the slope and the borehole lengths could be limited to 20–45 m. The boreholes were drilled in 2006–2008, since then, readings have been carried every two months by removable sliding inclinometer probe.

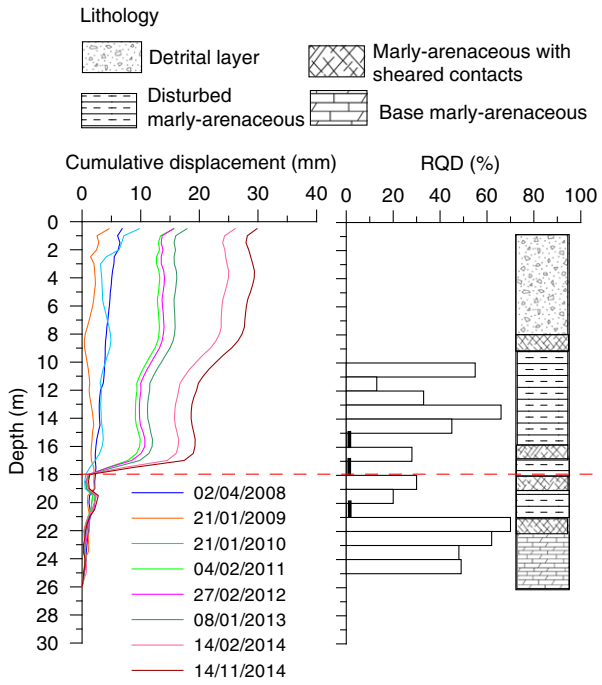

Fig. 4. Profiles of horizontal displacement vs depth from inclinometer measurements in borehole S27 (zero reading on 5/2/2007); RQD diagram and borehole stratigraphy.

4. Geotechnical investigations

The complex structure of the rock mass, as expected from the geological desk studies, was clearly confirmed by the analysis of borehole loggings (e.g., borehole S27 in Fig. 4). Borehole investigations have been focused on the N sector, particularly, in the zone of tunnel intake.

The bedding planes exhibit different orientation and texture in the upper and lower portion of the ridge, especially on the W flank, as already recognized from field surveys. This situation suggests that the entire body of the ridge can be divided in several zones, characterized by a different degree of fracturing and disarrangement of the rock mass (compare Fig. 2a, b and c). Data from borehole loggings are somewhat sparse, yet, it can be estimated that the chaotic structure typically accounts for 10 to 40% of total borehole loggings (Fig. 5).

The analysis of joint dips from borehole loggings (Fig. 6) shows that bedding and crossing joints are inclined, respectively, between 5–20° and 30–60°. Joint spacing lies in the 0.05–0.5 m range, as shown in Fig. 7. In the upper Marly-Arenaceous formation, joint spacing is

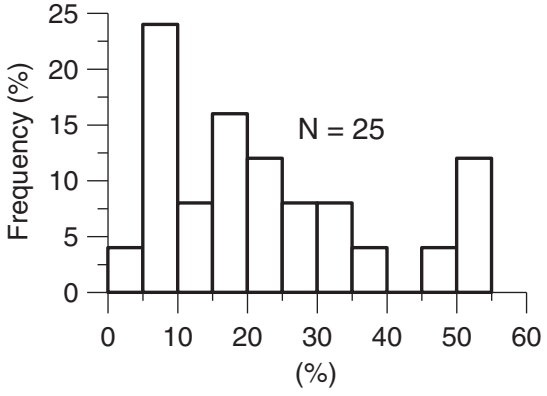

Fig. 5. Frequency distribution of the percentage of chaotic formation observed in 25 boreholes.

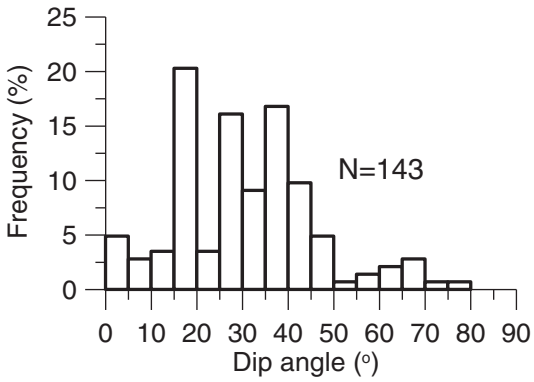

Fig. 6. Frequency distribution of joint dip angles (from 143 local measurements in different boreholes).

Fig. 8. Clay gouge interbed exposed in the damaged tunnel section; the thickness of the clay layer is approximately 0.2 m; on the left, a deformed steel set is visible.

typically 0.05–0.2 m while in the lower portion, less disturbed, it increases to 0.1–0.4 m.

For instance, the S3 borehole, drilled through the toe of the N slope of the ridge, shows that the Marly-Arenaceous-calcarenitic unit has RQD values are in the 40–70% range with average joint dip of 18–20°, while in the upper layer of disturbed marl the RQD values are in the 15–40% range and the joint dips are more dispersed, with typical values of 12–20°. Lower RQD values, in the 10–40% range, and even null values have been measured in the more disturbed zones, generally interpreted as the zones of more intense shearing. For instance, the borehole S27 (Fig. 4), located in the NW side of the ridge, shows RQD values of 50–70% for the undisturbed Marly-Arenaceous-calcarenitic unit and RQD of 15–30% at the depth of the shear zone.

4.1. Mechanical properties

The aspect of the cataclastic material (clay gouge) in the shear zone was examined from the exploratory window opened in the damaged portion of the tunnel, where the slip surface intersects the tunnel axis. The core of the shear zone consists of a 0.15–0.20 m thick band of laminated clay gouge (Fig. 8) entrapping small fragments formed by grinding of the rock walls (formed mainly of marl and sandstone) on the opposite sides of the slip plane.

The index properties of the clay gouge samples are: Clay = 46%, Silt = 45%, Sand = 9%, γ_s = 27.2 kN/m^3, w_L = 72.6%, w_P = 40.2%, PI = 32.4%, $CaCO_3$ = 20.1%. Therefore, the gouge material, with a largely prevailing silt and clay portion, can be classified as a high plasticity clay. The results of shear box tests in drained condition are: cohesion and friction at peak, c_p = 21.5 kPa and φ_p = 15°, residual friction, φ_r = 7.7° (Fig. 9). The intense shearing deformation occurred along the basal plane of the slope suggests that the mobilized strength is likely to be very close to residual conditions for most of the sliding surface.

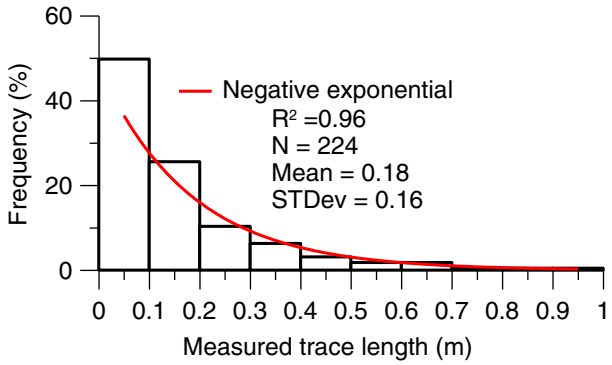

Fig. 7. Histogram of joint spacing measured in boreholes S28, S29, S1 and others.

The strength properties of the different rock materials have been obtained mainly by point loading tests. The unconfined compression strengths (UCS) of the marl and sandstone lithotypes are 22–88 MPa and 73–140 MPa, respectively. The rock joints are characterized by JCS = 30–40 MPa and JRC = 3–5.

Slickensided joints are frequently found in borehole cores (Fig. 10), mainly at the contact between marly and arenaceous layers, but also within claystone beds. Typical friction angles (Fig. 11) from in situ shear tests on slickensided and laminated bedding joints of the Marly-Arenaceous formation are in the range of 12–15° (Baldovin, 1968; Oberti et al., 1986). However higher friction angles between 26 and 35° have been reported by Oberti et al. (1986) for not-sheared contact planes between the sandstone and marly layers. The aforementioned large scale tests were carried out at different sites, within the same Marly-Arenaceous Formation.

Laboratory shear strength tests on clay-filled joints in limestone were conducted, for instance, by Hatzor and Levin (1997). In situ and laboratory shear tests by Alonso and Pinyol (2014) gave similar peak and residual strength, approximately 14°, for sandstone – sandstone contacts; while φ_p = 19° and φ_r = 13–18° for sandstone–claystone contacts. Grana and Tommasi (2013) report φ_r values dispersed in the 10–26° range, from ring shear test performed on specimens trimmed from an outcrop of the Marly-Arenaceous in a nearby site, also containing thick clay interbeds. Finally, ring shear tests of Tommasi et al. (2009) showed φ_p = 13–27° and φ_r = 10–15° for different types of clay-rich interbeds.

To complement the rock mass characterization, it was also considered the use of the common rock quality indexes, especially for the assessment of overall stiffness properties. For the disturbed zones of the rock mass, a GSI value of 25–35 can be assumed, while for the regularly bedded "bedrock", i.e., below the shearing zone at the base of the slope, a GSI of 45–60 can be estimated. The GSI-based estimate (Hoek and Diederichs, 2005) of the rock mass stiffness, taking the UCS influence also into account, gives an elastic modulus of 2–5 GPa and 5–10 GPa for the two typical conditions of the rock mass (regularly bedded and disturbed, respectively). Similar results can be found using the Q-value method (Barton, 2002).

The typical volume of the rock blocks can be estimated using joint frequency from scan-line mapping (Cai et al., 2004). Palmström (2005) suggested the use of a weighted jointing measurement on drill cores to approximate the volumetric joint count. But, if a sparse jointing is encountered, the average block size can be more effectively determined from the RQD values (e.g., Stavropoulou, 2014). Accordingly, the block volume can be estimated in the range of 0.5–3 × 10^{-3} m^3 for the disturbed rock mass and 5–30 × 10^{-3} m^3 for the bedrock.

Cross-hole seismic tests up to 30 m depth were performed in the past to assess the elastic properties of the dam foundation, entirely

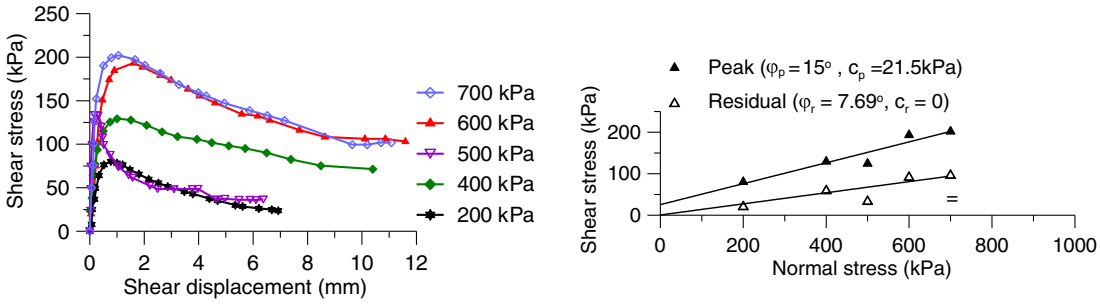

Fig. 9. Results of direct shear tests on clay gouge samples.

formed by alternate layers of sandstones, marl-clay and calcarenite of the a) unit. Fig. 12b shows the elastic parameters E_d and ν_d estimated from compression and shear wave velocities. A comprehensive study by Ribacchi (1987) on several dam sites in Italy shows a good correlation between elastic parameters obtained from plate loading tests and seismic measurements. Oberti et al. (1986) performed several plate loading tests on marly and sandstone units in a nearby dam site. Tests performed parallel and perpendicular to the bedding planes gave deformation moduli of 18–24 GPa and 16–18 GPa, respectively, which are slightly higher but practically comparable to the dynamic moduli measured at the Chiascio dam foundation.

Investigations performed on the N face of the slope (Fig. 12b) using down-hole and seismic refraction methods have shown that the P-wave velocity V_P is lower than 0.5 km/s in the first few meters, composed of loose debris (i.e., silt and gravel deposits). The P-wave velocity increases to 0.5–0.8 km/s in the disarranged portion of the Marly-Arenaceous formation and, finally, up to 3 km/s in the deep layers of sandstone and calcarenite.

4.2. Permeability tests and piezometer measurements

Lugeon tests have been routinely performed only in the area of the dam foundation, as required for the design and control of rock grouting works. The permeability of the rock mass (bedrock) lies in the 1×10^{-7}–3×10^{-7} m/s range (Fig. 13). Similar results were obtained by Oberti et al. (1986) for the Ridracoli dam foundation, with average permeability of 1×10^{-7} and 4×10^{-7} m/s at high and shallow depths, respectively. Less information are available for the disturbed Marly-Arenaceous formation in the slide area. According to the Barton (2002) empirical relationship, the permeability of the rock mass with lower P-wave velocity (0.5–1 km/s) would be in the range of 10^{-6}–10^{-5} m/s, considering Q-index values in between 0.01 and 0.1.

It is worthwhile to notice that the Marly-Arenaceous formation may exhibit higher hydraulic transmissivity in the direction of strata, with flow paths located preferentially along gaping discontinuities and more fractured sandstone strata, while the clay-rich layers essentially act as low-permeability barriers for flow in the direction perpendicular to the bedding.

To investigate the pore pressure distribution inside the slope, four deep boreholes were equipped with piezometer cells (Fig. 3). Each borehole hosts two Casagrande cells installed, respectively, above and below the presumed elevation of the slip surface. During the monitoring period the water level of the dam pool never exceeded 290 m a.s.l. Therefore, it can be said that the measured pore pressures have been mainly influenced by rainfall and infiltration.

5. General hypotheses and kinematic characters of the movement

5.1. Geometry of the sliding mass

Borehole investigations and survey of the N sector of the movement have shown that a basal slip plane can be reasonably assumed at the top of the buried alluvium layer. The displacement profiles of inclinometer verticals can give further support to this assumption.

The density of the geodetic targets is higher on the N slope and decreases in the S sector, at greater distance from the river bed. Anyhow, magnitude and direction of the horizontal displacements measured at the different monitoring points, even far away from the slope toe, are generally similar and consistent (Fig. 14). The average trend of the displacement vectors is approximately parallel to the longitudinal

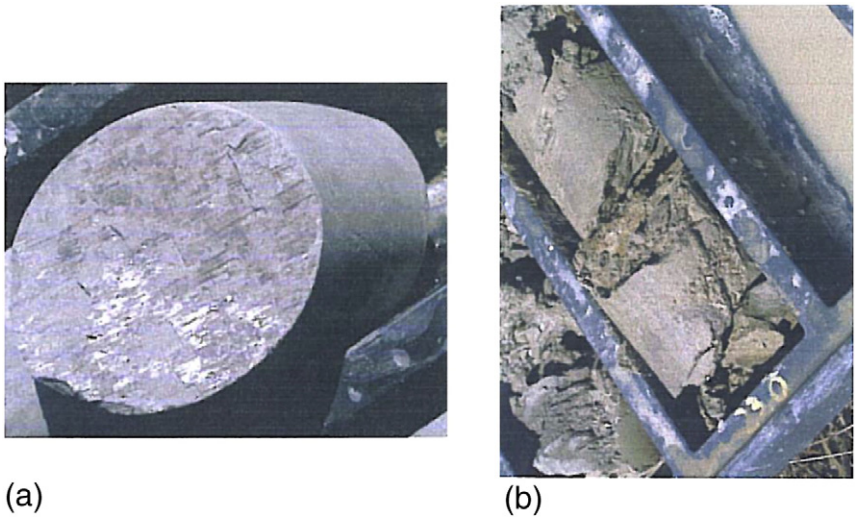

Fig. 10. Typical aspect of joint surfaces: slickensided joint recovered from borehole S27 at depth of 7.4 m (a), marly rock cores from borehole S3 at a depth of 25 m (b), near the slip surface.

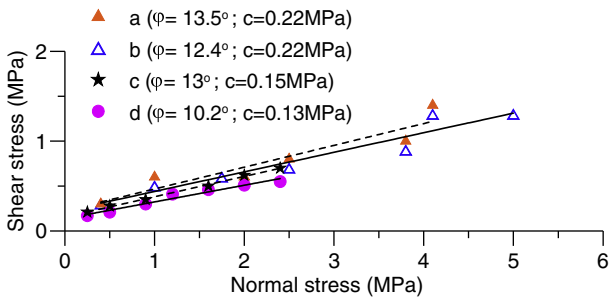

Fig. 11. Results of in situ shear tests performed on laminated joints, mainly between sandstone and marlstone layers, at different sites in the Marly-Arenaceous formation: a and b, data from Oberti et al. (1986), c and d, data from Baldovin (1968).

direction of the ridge, with some eastward rotation of the vectors at the toe of the slope. The basic hypothesis of a planar sliding with some internal shearing of the moving body seems therefore reasonable.

The position of the damaged tunnel section represents a further restraint to trace a likely longitudinal profile of the slip surface (Fig. 15). Finally, the upper limit of the movement (S boundary) was determined mostly on the base of the morphology of the ridge, i.e., by observing the presence of a plateau with some deformation traces at elevation 400 m a.s.l. The distance from this plateau to the river bed, measured along the longitudinal axis of the ridge, is approximately 1000 m.

The inclinometer measurements confirm that the slip surface can be reasonably drawn as a near horizontal plane in the toe part of the movement (Fig. 16). The slip surface is certainly more inclined in the upper part but the effective geometry cannot be defined in detail. This last issue will be further investigated also by comparing the results of different DEM models (see Section 6.1.3).

The lateral boundary of the movement can be traced more confidently on the E side, on the base of the displacement measurements, while on the W side the separation line between stable and unstable zone fades away (Fig. 14). The boundary of the movement is close to the top of the dam but the deformation does not affect the abutment zone, as demonstrated by the null displacement of targets N12 and N19.

The current kinematics of the movement can be outlined as a compound mechanism in which a block system is sliding on a low inclination basal plane. The depression along the surface profile of the ridge, between the targets N7 and N8 (Fig. 3), may represent a morphological evidence of past inter-block deformation. Inclinometer measurements can give a detailed description of shear strain distribution along depth, but they are available only for the toe zone of the slope. The deformation profiles generally show a rigid mass type of movement, with a clearly defined slip plane (e.g., Fig. 4), but in some cases a smeared deformation mode is also observed. It is apparent that most of the inclinometer measurements (Fig. 16) are consistent with the hypothesis of a flat basal shearing surface located at an average elevation of 267 m a.s.l., for the toe zone.

5.2. Time history of displacements

The time history of displacements measured for the geodetic targets (Fig. 17) shows that the ongoing deformations are characterized by an almost stationary velocity. Apart from the much higher velocities recorded in 1991, during the temporary operation of the diversion tunnel, the average velocity of the targets lies in the 13–17 mm/y range in the period 1992–2001 and tends to decrease in the following years. However, temporary increases in velocity have been observed also in the last years, particularly for the 2014 measurements. The tunnel extensometer exhibits a similar trend and a consistent magnitude of total displacement.

A secondary cyclic fluctuation in velocity is also evident, particularly for the displacements measured on the surface of the slope. This behavior is a likely consequence of transient seasonal variations in groundwater pressure and temperature. Additional difficulties in analyzing the velocity histories (Fig. 17) stems from the low frequency of measurement. Some targets also show alternated phases of negative and positive velocity, which may be tentatively explained as the combined effect of "stick-slip" phenomena and water content / temperature variations.

5.3. Pore pressure regime and rainfall influence

The average profile of the water table, as shown by the piezometer measurements in borehole A, B, C and D, progressively decreases towards the toe of the slope (Fig. 3). The two piezometer cells in the uppermost borehole (cells D1 and D2), placed at a depth of 80 and 97 m, respectively, have recorded null pressures for most of the measurement period. The remarkable difference in piezometric head between cells in the same vertical (particularly for the vertical A and C) suggests

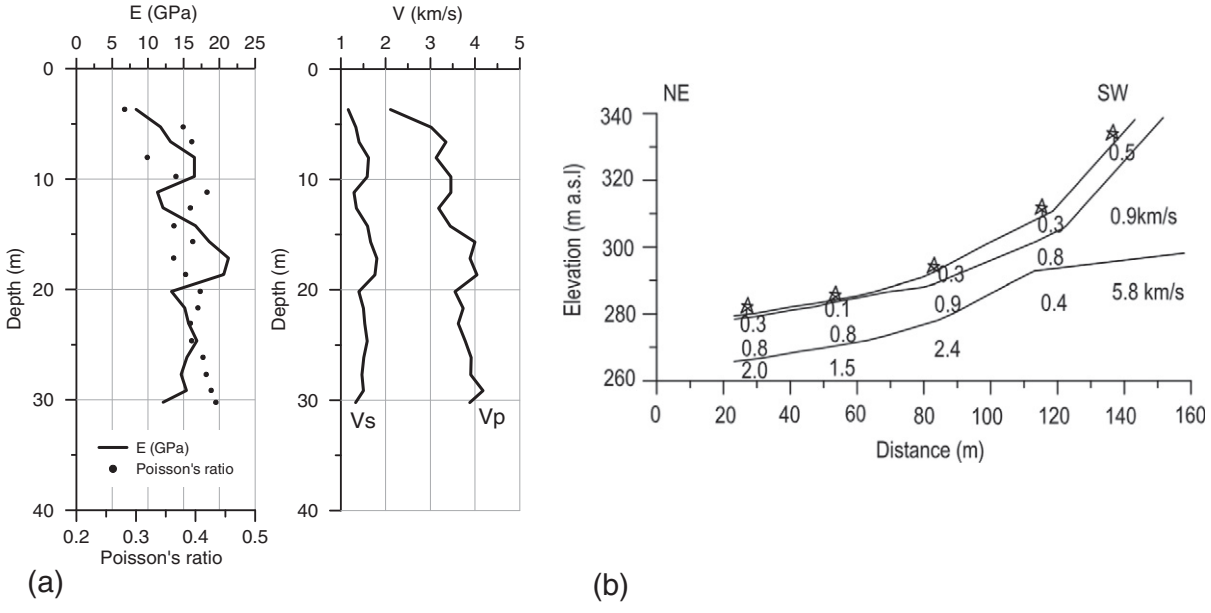

Fig. 12. Results of cross-hole tests in the dam foundation, in boreholes A-B (a), and P-wave velocity distribution from seismic refraction (line P15) at the slope toe (b).

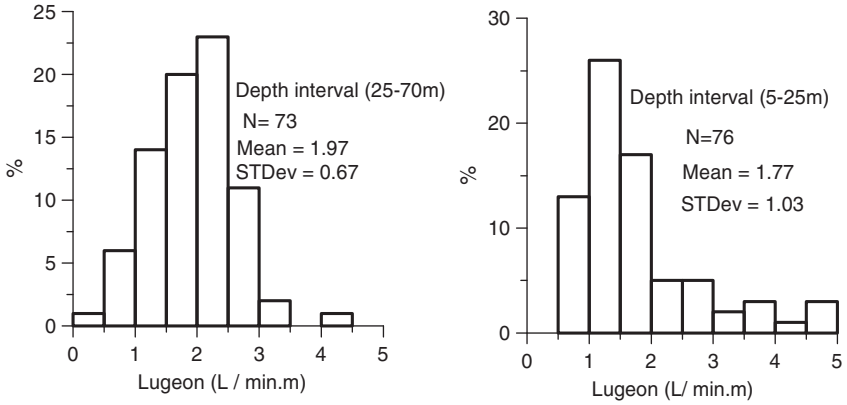

Fig. 13. Frequency distribution of Lugeon values from tests performed in different boreholes located in the area of dam foundation.

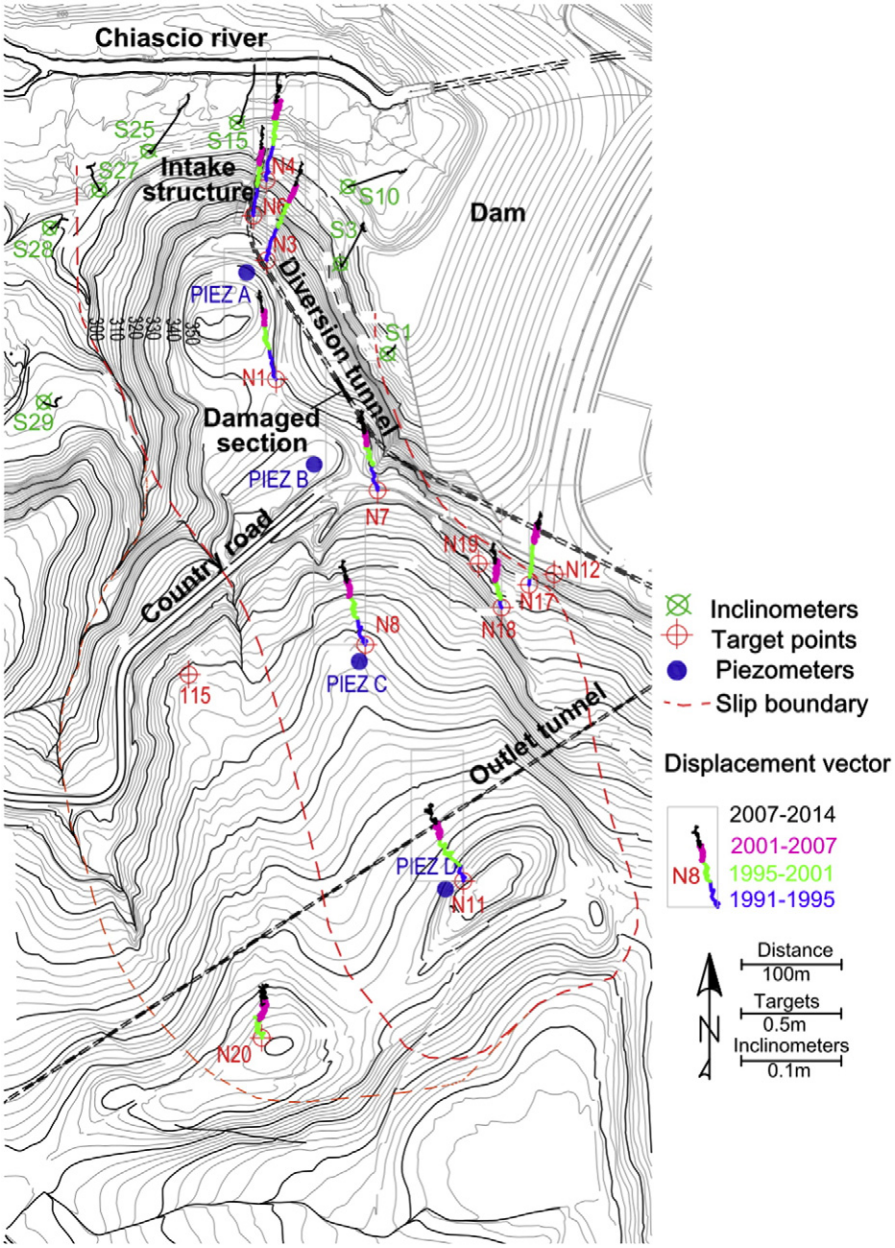

Fig. 14. Plot of horizontal displacements and boundary of the movement.

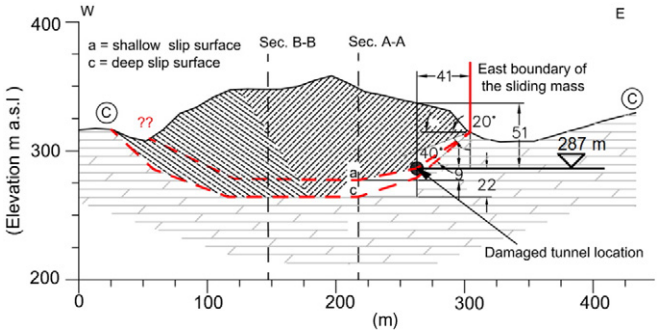

Fig. 15. Transversal section of the ridge with the slip surface reconstructed considering the position of damaged tunnel and the typical dip angles (20–40°) of bedding planes at the East boundary (all dimensions are in m).

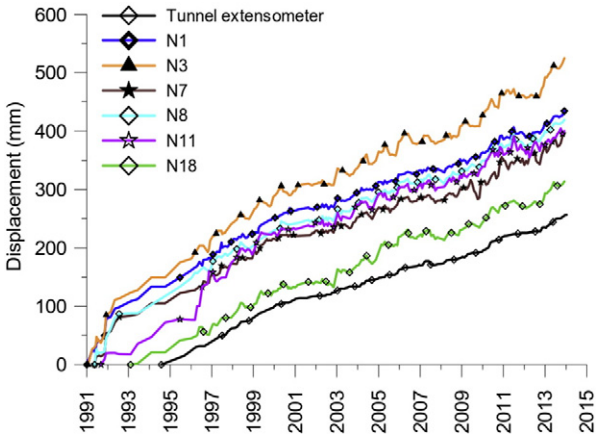

Fig. 17. Displacement histories of the geodetic targets and of the telescopic joint of the tunnel; the time of the first measurement is not the same for all the monitoring points.

complex conditions of groundwater flow within the slope, in which fractured rock aquifer layers are alternated with less permeable (marly) layers. Readings from piezometer B2, located in the same area of the damaged tunnel section, show a local falling in the groundwater table, which can be tentatively explained as the effect of a local increase in permeability, related to the higher degree of loosening of the rock mass in this sector of the ridge. The local morphology of the slope may also have some influence, in fact, the steep flanks of the ridge facilitates the drainage process in transversal direction.

The maximum fluctuation of groundwater levels around the average value is around 10 m. The time-lag between pore pressure increases in piezometers and rainfall was also analyzed. Peaks in piezometer levels seem best correlated with the 3-month cumulated rainfall, particularly for rainfalls exceeding the average seasonal trend (Fig. 18). Correlation analyses were also attempted between displacement velocities and rainfall, but the interpretation of the results proved to be particularly difficult due to the low frequency of the measurements (Fig. 18).

6. DEM modelling of the slope

The initial aim of the DEM (Distinct Element Model) modelling of the slope was to investigate the influence of the structure of the sliding mass (i.e., geometry of slip surface and joint pattern) on the deformation mode and on the mobilized strength of the slip surface. A 2D discontinuum modelling approach was adopted via the UDEC code (Itasca, 2011). The rock blocks are formed by linearly elastic material while the joint behavior is ideal elasto-plastic with Mohr–Coulomb strength criterion.

The following analyses represent primarily a back analysis of the slope deformation observed in more than 20 years of field monitoring, which has allowed to classify the movement as a "slow" deformation. Dynamics aspects, often included in the analysis of catastrophic failures

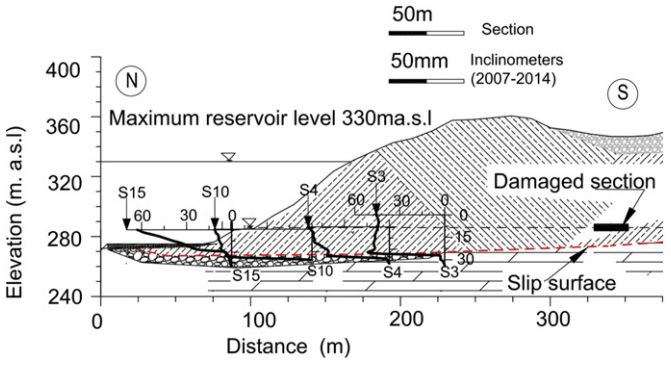

Fig. 16. Shape of the slip surface traced at the toe part of the slope on the base of inclinometer profiles.

of slopes (e.g. Kveldsvik et al., 2009; Alonso and Pinyol, 2010), are not relevant for the present case. The conventional local damping approach, implemented in the UDEC code for the analysis of static or quasi-static deformation processes, can be therefore, reasonably applied.

The Chiascio slope has been modelled as a complex blocky structure defined by several joint sets (Fig. 19). Note that the model in Fig. 19 (Model A), characterized by fully continuous joints, represents only one of the candidate modelling options. For sake of simplicity, the general features of all the DEM models are herein presented by making reference to this specific case.

The cross section of the slope considered for modelling is parallel to the longitudinal axis of the ridge. The bedding planes (joint set 1), gently inclined and markedly continuous, are crossed by sub-vertical joints (joint set 4) and secondary crossing joints (joint set 2 and 3, with intermediate dip angles and opposite dip direction). The dip angles of the last

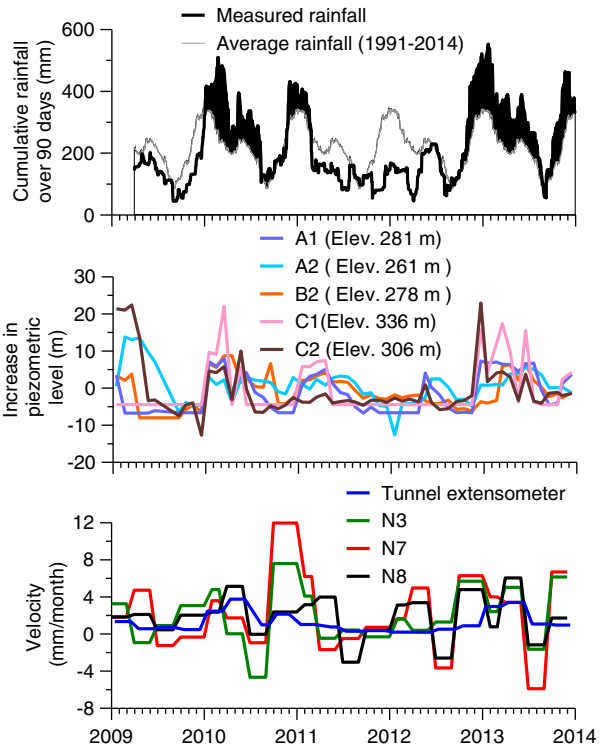

Fig. 18. Comparison of excess rainfall (shaded area), increase in piezometer level and displacement velocity histories. Note that the increase in piezometric elevation is relative to the average value; in the period 1994–2014.

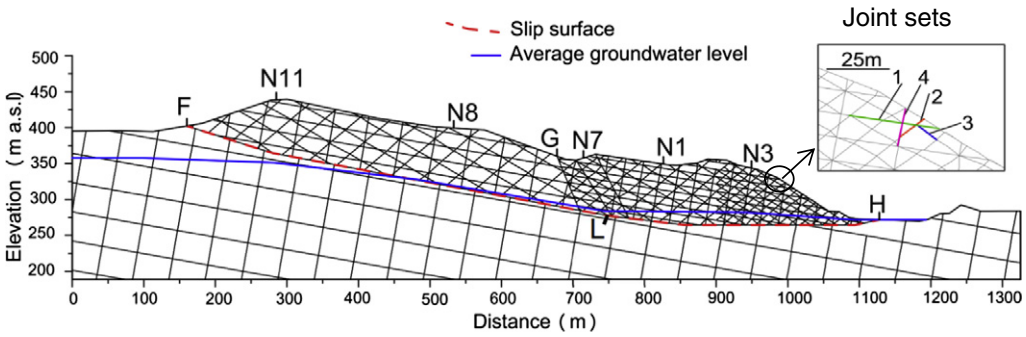

Fig. 19. Model A with continuous joint pattern.

joint sets, 40° and 30° respectively, correspond approximately to the modal values of the statistical distribution of measured inclinations (Fig. 6). The role of the joint sets 1 and 4 is essentially to reproduce the "regular" blocky structure typical of the less deformed portion of the slope, while the joint sets 2 and 3 represent the superimposed "disturbed" texture due to tectonic and recent deformations. The joint spacing has been reduced in the more disturbed portions of the slope, i.e., at the toe and in the transition zone. This last zone corresponds to a diagonal band, traced between points G and N7 in Fig. 19, where the dip angle of the basal slip changes.

The mechanical properties of the joint sets are shown in Table 1. All the joints have been given the same normal and shear stiffness; and purely frictional strength. The normal stiffness of the joints (k_n = 2.3 GPa/m) has been calibrated so that the equivalent rock mass modulus is in agreement with the elastic modulus suggested by the GSI approach and the dynamic modulus derived from cross-hole seismic investigations (see Section 4.1). This approach has been often adopted (e.g., Zhang and Einstein, 2004; Kulatilake and Shu, 2015); in the present case, it was specifically applied for the calibration of joint normal stiffness k_n for the less disturbed rock mass. Then, the overall stiffness for the other structural domains (i.e., bedrock, transition zone and disarranged zones of the rock mass) was tuned by varying only the joint spacing. The shear stiffness of the joints k_s has been assumed equal to 0.1 k_n, a common assumption derived from typical experimental results. The Young modulus E of the material forming the individual blocks is 4 GPa, irrespective of the variability of lithotypes; which clearly represents an idealized situation.

The choice of joint strength parameters in DEM models is a particularly complex issue, because strength and geometrical properties (e.g., block shape, joint pattern) are generally inter-related and scale-dependent. In the case of the Chiascio slope, it was preferred to characterize the joint strength by a single parameter (the friction angle) and assume a dilatancy angle equal to zero for all the joint sets. The friction angle of the bedding planes directly stems from in situ shear tests (18°), while the friction angle assumed for the crossing joints must be considered a "design" value (30°), i.e., it is the minimum friction required to avoid unrealistic failure mechanisms, significantly lower than the characteristic strength of the undisturbed, not sheared, crossing joints. This last point will be discussed in Section 6.1.2.

The reasons for neglecting the dilatancy effect are different for the different joints. It is a physical evidence for the laminated clay gouge of the slip surface and the slickensided bedding joints, found especially in the more disturbed zones of the slope. It can be considered a model simplification for the crossing joints.

The influence of a different degree of shearing, interlocking and disarrangement of the crossing joints will be analyzed, not varying the strength and dilatancy parameters but modifying the joint pattern (continuous or staggered) and spacing (decreased in disturbed zones). Particularly, the "brick-wall" arrangement of rock blocks, implemented in Model B (Fig. 21), can be viewed as an alternative approach to model the increase in interlocking effect caused by dilatancy of cross joints.

In the DEM approach implemented in UDEC, blocks are impermeable but water pressures are considered for the constitutive model of the joints. Water pressures can be initialized, for a purely mechanical analysis, simply by assigning the water table profile. The joint aperture (initial and residual), provided in Table 1, was utilized only for the flow analyses of Section 6.2. The typical aperture of bedding planes in arenaceous units and interfaces between arenaceous and marly layers is about 1 mm, but the situation is very variable, particularly for the cross joints in the disarranged zones of the rock mass. The joint aperture parameters reported in Table 1 will be discussed in Section 6.2.

The present morphology of the slope has been obtained, in the DEM models, by the simulation of an "erosion" process, starting from an ideal initial situation in which the ground surface is horizontal and horizontal-to-vertical stress ratio is 0.5. The reference groundwater table of Fig. 19 represents the average profile obtained from piezometer measurements (boreholes A, B, C and D).

Table 1
Joint properties adopted in UDEC simulations.

Description	Spacing[a] S (m)	Dip angle y (°)	Friction angle φ (°)	Normal stiffness k_n (GPa/m)	Shear stiffness k_s (GPa/m)	Initial[b] joint aperture a_0 (mm)		Residual[b] joint aperture a_{res} (mm)	
						U	L	U	L
Bedding planes (1)	8–16	10	18	2.3	0.23	0.5	2	0.5	1
Joint set (2)	12–24	40	30	2.3	0.23	1	2	0.5	1
Joint set (3)	10–20	30	30	2.3	0.23	1	2	0.5	1
Joint set (4)	20–40	80	30	2.3	0.23	1	2	0.5	1
Slip surface	–	Varies[c]	Varies[d]	2.3	0.23	1	2	0.5	1

*Joint aperture in column-U are for upper portion between F-G while in column-L are for the lower part between G-H.
[a] Spacing is different for the upper and lower (transition and toe) portions of the slope.
[b] Initial and residual apertures are utilized for flow analyses by the DEM model.
[c] A range of dip angles of the slip surface (c) is considered for the model in Fig. 19.
[d] Friction angle of the slip surface is varied according to the shear strength reduction method.

The study was initially focused on the influence of the rock mass structure on the deformation mode and failure conditions of the slope. The limit friction angle of the slip surface, for a given joint pattern, has been obtained by the Strength Reduction Method (SRM) (e.g., Dawson et al., 1999). To this aim, the unbalanced forces ratio, set equal to 10^{-6}, was adopted as the basic convergence criterion (Itasca, 2011). Additionally, the displacement history of several grid points was also monitored. The selected control points correspond to the position of some geodetic targets (N1-N11) located on the top of the ridge.

As highlighted by previous studies (e.g., Boon et al., 2014), capturing the strength limit which corresponds at the onset of collapse involves some computational difficulties. The expedient of progressively decreasing the step-size for strength reduction as the system approaches the failure limit has proven useful to reduce dynamic disturbances and attain a smooth response of the system. Specific calculation tests have shown that the reduction step for the friction angle of the slip surface must be less than 0.6° in order to progressively mobilize a basal slip failure, otherwise, random loss of contact of single blocks and local instability may occur.

In some cases, it is relatively easy to identify a critical threshold in the "mobilized friction vs displacement" curve obtained from the SRM, i.e., to identify a limit value of the friction angle corresponding to a sharp increase in displacement. For instance, this is the case of the simple model in Fig. 20, for which the critical threshold can be localized at $\varphi = 8°$ (point of maximum curvature on the response curve).

In other cases, particularly for models having a more complex blocky structure (see for instance Fig. 22), it has been found that the response curve ("mobilized friction vs displacement" curve) may exhibit a less sharp knee which, for further decrease in friction, leads to displacement increments progressively larger but yet compatible with overall equilibrium conditions . Therefore, it was deemed useful to consider also a second critical value for the mobilized friction, i.e., the friction angle corresponding to the "threshold of large displacement". For the DEM models of the Chiascio slope, this threshold has been assumed in the order of 3 m.

The aforementioned criterion may be considered purely empirical and not fully satisfactory, but has proven effective, at least to compare the response of different models and assess the impact of different loading conditions.

6.1. Influence of the blocky structure of the slope

6.1.1. Block size

Since the joint spacing of the model must be increased with respect to the real situation, to get a reasonable number of blocks for modelling, it is necessary to analyze the influence of block scaling (Zangerl et al., 2003; Boon et al., 2014). The effect of block size has been investigated by comparing the mechanical response of two simplified models in which only two joint sets, (1) and (4), are implemented with spacing S and 0.5*S, respectively (Fig.20).

The results of Fig. 20 show that block scaling affects the overall stiffness of the rock mass, obviously, but the limit friction angle of the slope does not change significantly. The block size was further decreased (1/3 of block size shown in Fig. 20a) and the former results were confirmed again. Similar findings were obtained by Boon et al. (2014), who noticed that the failure friction angle is progressively less sensitive to block size as the number of blocks becomes sufficiently higher.

For the models shown in Fig. 20, as the number of blocks increases the model exhibits not only a basal sliding but also significant shearing along the sub-vertical joints and secondary toppling deformations in the frontal part of the slope may occur.

6.1.2. Joint pattern

A first set of analyses were performed with the model of Fig. 19 (Model A), in which all the joint sets are continuous. After the considerations of Section 6, it was decided to implement also a model with staggered joint (Model B in Fig. 21). The "brick-wall" structure of this model is generated by the intermittent joint of set 4.

Preliminary numerical tests were carried out for different values of the friction angle of the crossing joints. Different failure mechanisms of the slope could be observed. The shear strength properties for the joint sets were finally decided on the basis of the model response, particularly for the joints set 3 and 4 (Fig. 19). In fact, it was found that, in order to mobilize a sliding failure along the basal slip surface, a minimum friction angle of 30° was required for the cross joints of Model A and B. For friction angles lower than these, completely different collapse mechanisms were observed, not in agreement with the actual kinematics of the movement, i.e., the sliding failure of rock mass wedges along joint set 3 in the frontal zone of the slope (between points N3 and H in Fig. 19).

Furthermore, preliminary analysis has shown that relatively lower friction angle can be sufficient for the cross joints of Model B in order to mobilize the observed deformation mode.

Therefore, the 30° friction angle can be interpreted as an overall strength parameter, which includes the interlocking effect of the non-persistent joints, particularly for Model A. Moreover, it was found that higher values of the cross joint friction angle have negligible influence on the critical strength of the basal slip.

Model B with staggered joints exhibits less internal shearing of the sliding mass and a more uniform distribution of horizontal displacements. The pre-failure deformation of Model A is more complex: the lower portion of the slope, e.g., points N1 and N3, moves slightly more

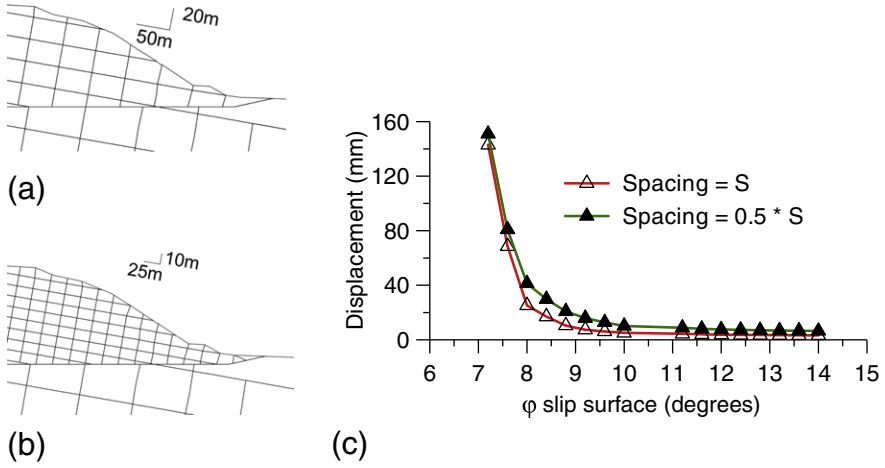

Fig. 20. Detail of the models with joint spacing S (a) and 0.5*S (b); calculated displacement of point N3 vs mobilized friction angle of the slip surface (c).

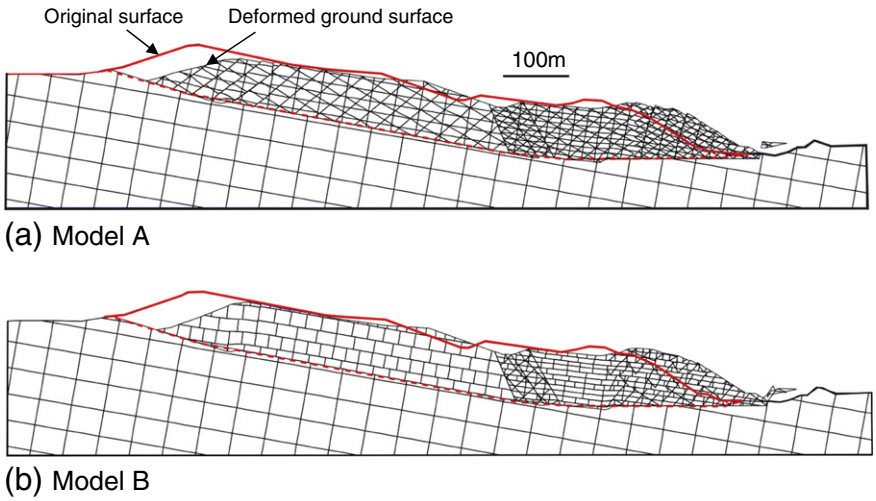

Fig. 21. Deformed shape (magnification factor: ×400) of Model A (a) and of Model B (b) for a mobilized friction angle $\varphi = 8°$ on the basal slip surface.

than the upper portion (Fig. 21), where shearing deformations along the joints dipping towards S (joint set 2) are also activated. A similar influence of the joint pattern on the internal deformation mechanism was reported in some previous studies (e.g., Hammah et al., 2009; Brideau and Stead, 2012).

For both models, plastic shearing along the basal slip starts up when φ is reduced to 8.4° (Fig. 22). Then the displacement increment is slightly lower for the model with staggered joint (Model B). The increase in displacement is of the same magnitude for all the control points (from N3 to N11), thus demonstrating that the longitudinal stretching of the sliding body is impeded by interlocking, with the exception of the uppermost zone of Model A.

The limit friction angle (maximum curvature point on the response curves of Fig. 22) is practically the same for Model A and B: it is equal to 7.6° and therefore almost coincident with the residual friction angle obtained from the shear box tests on clay gouge. In the light of the Strength Reduction Method, it can be also introduced a Safety Factor (S.F.) of the slope, calculated as the ratio of the tangent of the actual mobilized friction angle to the tangent of the "failure" friction angle. The S.F. reported in Fig. 22 has been calculated with respect to the previously defined limit value ($\varphi_{lim} = 7.6°$).

The deformation mode of the blocky system can be better visualized after a further small reduction in the friction angle ($\varphi = 7.2°$) of the basal slip surface (Fig. 23). Large slip displacements along the basal plane are accommodated by inter-block displacements throughout the entire thickness of the sliding body.

For both models the internal deformations are localized in the transition zone and around the point where the inclination of the basal plane changes, but the deformation mechanism is quite different. While in Model A the overall flexural deformation of the stacked layers is mainly the result of shearing along inclined joints, in Model B it is the combined effect of partial opening of transversal joints and interbed shearing. The latter mechanism represents the typical "ductile style" deformation for layered rocks. Similar features of the deformation mechanism can be noticed of the upper zone of the slide (sector of point N11). In Model A the internal shearing is mainly localized along the joints dipping to S (joint set 2 and 4).

6.1.3. Depth and shape of the slip surface

The field evidences available to delimit the unstable volume have been discussed in Section 5.1. It was concluded that depth and shape of the slip surface can be unambiguously defined only in the toe portion of the slope. However, several elements and restraints can help to trace also the upper part of the slip surface (Fig. 24a). In fact, i) it must intersect the damaged tunnel, ii) the transversal (West - East) cross section should be typically bowl-shaped, as suggested by the way the bedding inclination varies (see Fig. 15), iii) the upper limit of the slip, as well as the position of the so-called transition zone, are clearly indicated by morphological characters of the slope surface, iv) the essentially planar shape assumed also for the upper portion of the slip surface is again suggested by the general layout of the bedding, v) the inclination of the upper slip plane can therefore vary within a narrow range, with values similar to the average longitudinal slope angle of the ridge.

The four hypotheses a, b, c and d (Fig. 24a) implemented in the DEM model clearly reflect, and reasonably bracket, the aforementioned conditions. The blocky structure of the model is identical (with the joint pattern and spacing of Model A in Fig. 19 and 21a), only the profile of the slip surface, represented by a continuous chain of

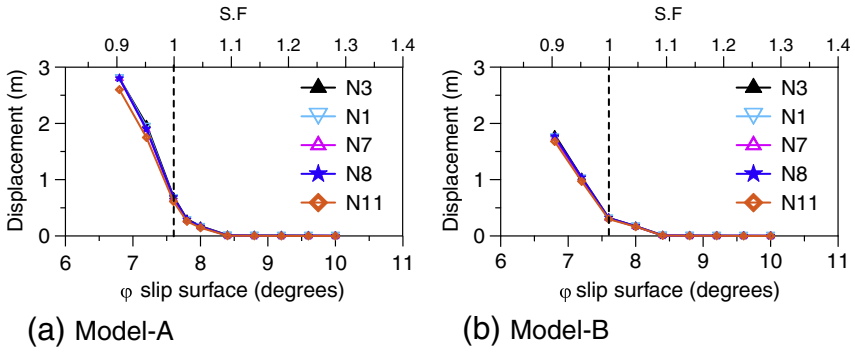

Fig. 22. Calculated displacement vs mobilized friction angle along the basal slip surface for Model A (a) and Model B (b).

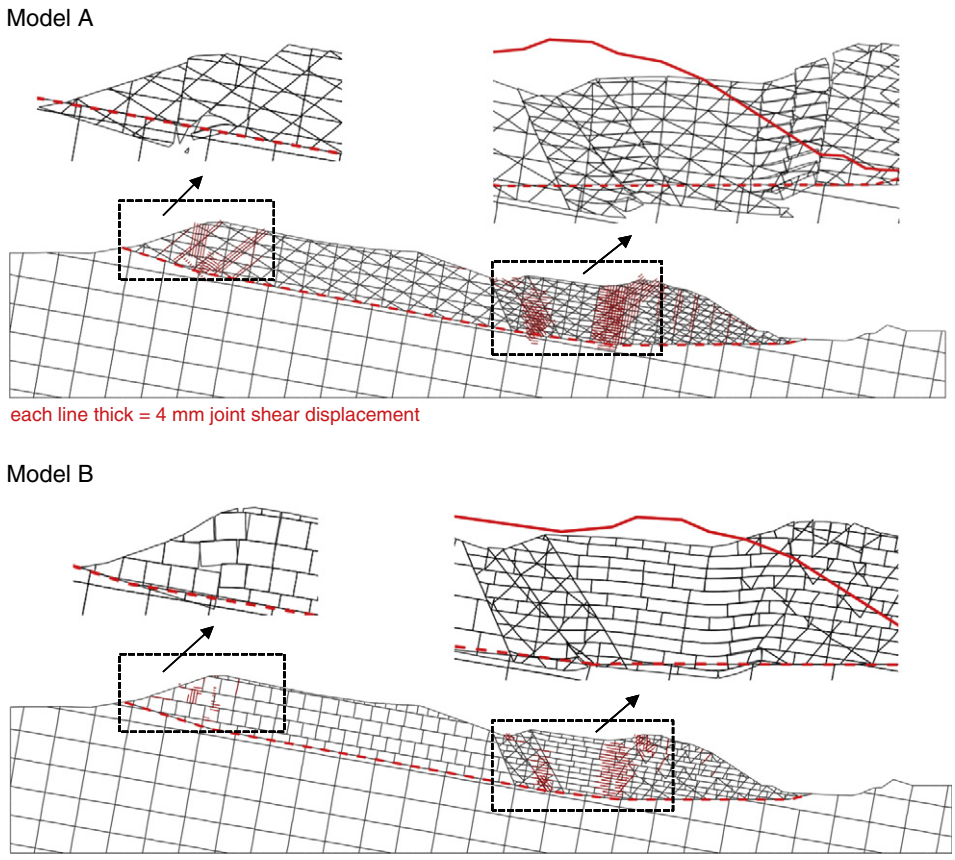

Fig. 23. Comparison of the calculated shear displacement along joints in Model A and B for a mobilized friction angle φ = 7.2° on the basal slip surface; details of the local deformation mechanism (magnification factor: ×100) in the zones of intense shearing.

linear cracks, is different. The dip angle of the upper portion of slip surface varies between 7 and 13° and, correspondingly, the overburden reduces from 100 to 54 m. The hypothesis (a), specifically, represents the case of minimum possible depth of slip, in agreement with a less concave shape of the transversal cross section of the slip surface (see Fig. 15).

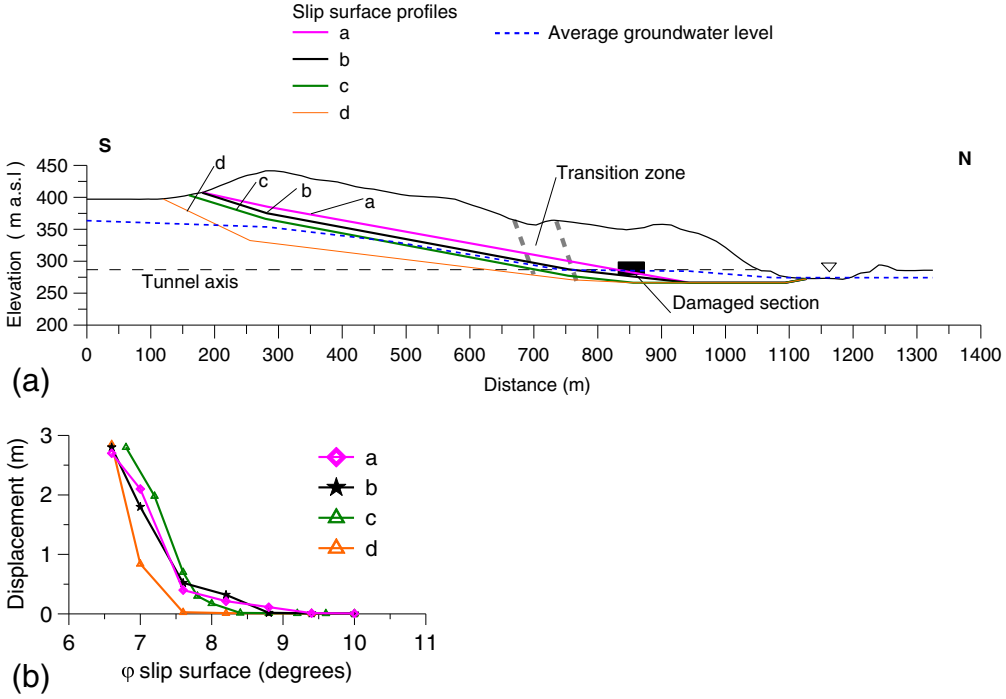

Fig. 24. Different hypotheses considered for the longitudinal profile of the slip surface (a); curves of displacement vs mobilized friction obtained for each case (b); note that the displacement plotted in the figure is the horizontal displacement of the control point N3 (Model A).

The horizontal portion of the slip surface is equal for profiles (a) and (b) and for profiles (c) and (d). For case (c), the limit of the horizontal slip surface corresponds to the boundary of the "transition zone", formerly identified on the base of morphological evidences on the ground surface. Case (d) is characterized by a deeper and less inclined slip surface in the upper portion, and a horizontal surface in the toe part.

Fig. 24b shows the curves of calculated displacement (point N3) vs mobilized basal friction for each model. The slip surface (c) is the same for Models A and B considered in Section 6.1.2. As already noticed, in this case the first plastic strains start for a friction angle of 8.4° and the conventional failure limit can be located at 7.6°. The slip surfaces (a) and (b) exhibit plastic deformations when the friction angle is reduced to $\varphi = 9.4°$ and 8.8°, respectively. A sharp increase in displacement (failure limit) occurs when $\varphi = 7.6°$ for both the slip surfaces (a) and (b). The surface (d) shows up the first plastic deformations for a friction angle close to 7.6°, a value significantly lower than in the other cases. For further reductions in mobilized friction, the response curve of the model with the deepest slip profile (d) exhibits very sharp increase in displacement increment.

The profile (c) was finally accepted as the reference case for the following analyses. The "armchair" shape of the slip surface entails intensified shearing of the joints in the transition zone, where the slip angle turns from the mild slope of the upper zone to zero (Fig. 24). This characteristic shape has been frequently observed in large slope movements, as the well-known case of the Vajont slide. Recent studies (Alonso and Pinyol, 2010; Yerro et al., 2015, among others) have highlighted the influence of localized shearing around the bending point of the slip, yet, in the present case the change in slope is smaller and less critical than in the Vajont case.

6.1.4. Influence of groundwater table and reservoir filling

In a first set of analyses, the water level of the reservoir is kept constant at 274 m a.s.l. (i.e., the reservoir is considered "empty"), while the groundwater table inside the slope is equal to the average (AGW) or maximum (MGW) level recorded throughout the monitoring period. The AGW as well as the MGW conditions have been implemented in the DEM model by the "water table" approach, which imposes a hydrostatic distribution of water pressure within each joint according to the local depth from the water table (Fig. 25a).

The AGW conditions represent the reference case, already considered in the previous analyses. As already observed, in this case, the first plastic deformations occur when the basal friction is reduced to 8.4° and the limit threshold of large displacement is at $\varphi = 7.6°$ (Fig. 25c). The raise of the water table to the MGW conditions changes the response curve of the slope significantly. In this case, plastic deformations occur since the friction angle is reduced to 9.2° and the second threshold is at $\varphi = 8.2°$.

In a second set of analyses the influence of the reservoir filling is considered. The water table is assumed horizontal throughout the intersection point with the average groundwater table profile (AGW). For the mobilized friction along the slip surface two hypotheses have been considered: in the first case the friction angle is constant (equal to 9°) throughout the entire length of the surface, in the second case the friction angle is reduced to 7.6°, but only for the flat portion of the surface (from point L to H in Fig. 25a).

The water level of the reservoir has been increased by steps of 5 m, up to the design maximum elevation of 330 m a.s.l. Fig. 25b shows the "rate" of increase in horizontal displacement predicted for the control points N3 and N8, for each step of reservoir rising. This "rate" is calculated as the ratio of the displacement increment divided by the increase in water level (in Fig. 25b it is measured in millimeter/meter).

The reservoir filling modifies the pore pressure distribution mainly in the lower portion of the slope, i.e., along the flat portion of the slip surface and throughout the transition zone. The effect of the water pressure increase within the joint systems is complex: in fact, the buoyancy effect (equivalent to a decrease in the total vertical force applied on the

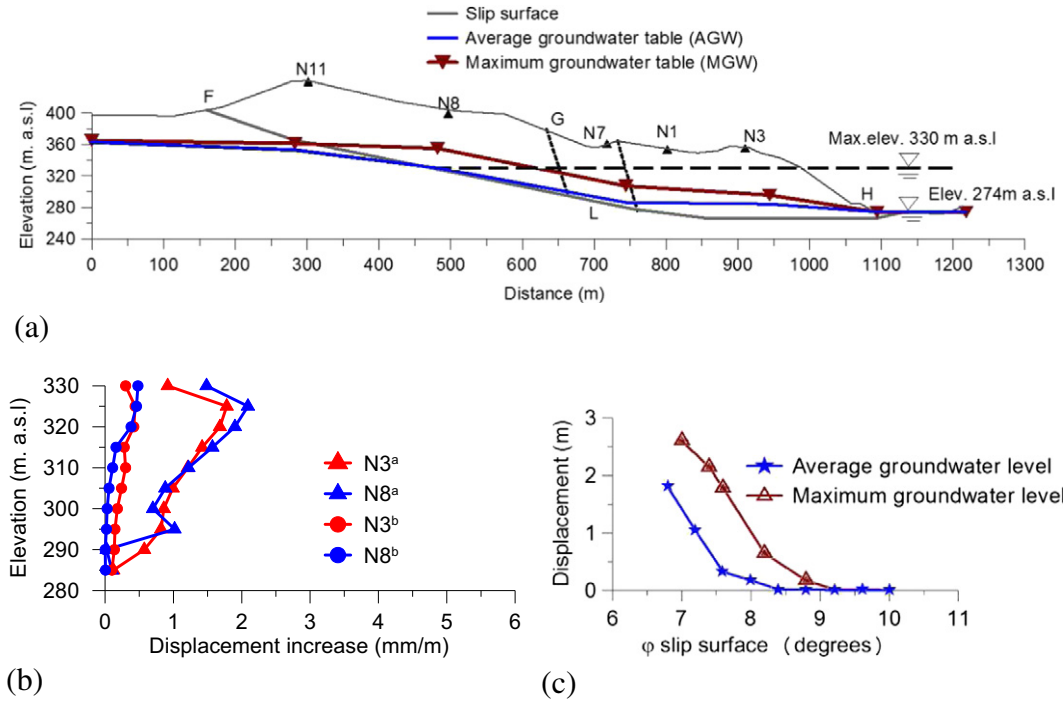

[a] displacement rate when the friction angle is equal to 9 and 7.6° for the upper part (F-L) and the lower part (L-H) of the slip surface, respectively.
[b] displacement rate when the friction angle is equal to 9° for the whole slip surface.

Fig. 25. Average and maximum elevation of groundwater table (from piezometer readings), maximum level of reservoir considered in DEM modelling (a); horizontal displacement increases calculated for the progressive filling of the reservoir, up to the design maximum level of 330 m a.s.l. (b); curves of horizontal displacement (N3) vs mobilized friction angle calculated for two different groundwater profiles (average and maximum) and empty reservoir (water level at 274 m a.s.l) (c).

rock block) is combined with the effect of the overall reduction in the pressure gradient in horizontal direction (equivalent to a reduction in the horizontal drag force applied on the rock block). It is worthwhile noticing that the "water table" approach, i.e., setting up a piezometric line and assuming a hydrostatic distribution of water pressure for each vertical, accounts for the aforementioned effects only approximately.

Fig. 25b shows a continuous increase in the displacement rate as the reservoir level is increased step-by-step up to el. 325 m, while a marked decrease is observed for the last calculation step, up to el. 330 m. The lower and upper portion of the slope exhibit a similar response, represented by the horizontal displacement of the control point N3 and N8, respectively. The vertical component of the displacement, not reported in the figure, is positive (upwards) in the lower part (from point H to G) and negative in the upper part (from point G to F). The horizontal displacement in N3 is generally higher than in N8, for both the situations, i.e., for $\varphi = 9°$ and $\varphi = 7.6°$ in the toe part of the slip surface.

It can be tentatively concluded from the previous results that the progressive filling of the dam pool does not cause an abrupt failure but a progressive increase in shearing along the basal joint. The response of the slope to the change in water pressure conditions will be discussed more exhaustively in Section 6.2, devoted to coupled flow analysis.

6.2. Hydro-mechanical analyses

The influence of water pressure distribution in the joint network has been further investigated by coupling the analysis of mechanical equilibrium with steady-state flow calculation. In these coupled hydro-mechanical analyses the hydraulic conductivity of joints depends on mechanical deformation and vice-versa.

The flow rate q in a joint element, between two points with water pressure p_1 and p_2, is given by the cubic law equation for laminar flow between two parallel plates with smooth surfaces (Witherspoon et al., 1980)

$$q = \frac{a^3}{12\mu} * \frac{\Delta p}{\Delta l} \quad (1)$$

where Δp is the net pressure differential $p_2 - p_1 + \gamma_w(z_2 - z_1)$, Δl is the distance between the two points located at elevation z_1 and z_2, respectively, a is the hydraulic aperture and μ the dynamic viscosity of water (10^{-3} Pa·s).

The hydraulic aperture a may change during the calculation steps, due to mechanical closure or opening of the joint; it is given by the following expression

$$a = a_o + u_n \quad (2)$$

where a_o is the initial hydraulic aperture, evaluated in geostatic conditions, u_n is the joint normal displacement (positive denoting opening) which depend on the variation in normal effective stress, joint stiffness and dilation. For the aperture a, it is assumed that below a minimum value, a_{res}, the mechanical closure does not affect the conductivity of the joint element.

In some preliminary analyses the aperture of joint sets in different zones of the model (i.e. the upper part of the slope, the transition zone and the toe) has been varied in order to investigate the effect of different distributions of permeability on the steady state water pressures. The initial aperture can be assumed in the 0.5 ÷ 1 mm range for the bedding planes and in the 1–2 mm range for the crossing joints.

Field evidences, particularly borehole loggings and seismic velocity measurements, suggest that the more disturbed rock mass forming the lower part of the slope, including the transition zone (i.e., from point G to H in Fig. 26), should be given a higher permeability compared to the less disturbed rock mass in the upper part.

Hints of somewhat different flow conditions in the transition zone come from the analysis of piezometer measurements in the borehole B: i.e., the piezometric line seems to show a local fall in the zone of borehole B. This fact can result from different causes: a local increase in permeability but also the effect of a flow component (perpendicular to the model plane) directed towards the steep E and W flanks of the ridge. Therefore, to account for the aforementioned effects, relatively higher apertures, $a_o = 2 \times 10^{-3}$ m and $a_{res} = 1 \times 10^{-3}$ m, have been assumed for the joint sets in the lower portion of the model (between the point G and H, including the transition zone). Table 1 reports the final decision about the joint apertures for the different zones of the slope model.

The hydraulic boundary conditions on the vertical edges of the model are representative of the average situation during the 25 years of geotechnical monitoring (i.e., empty reservoir). The hydraulic head on the right boundary corresponds to the average elevation of the Chiascio river (274 m a.s.l.) while on the left boundary the hydraulic head has been fixed at 364 m a.s.l. by extrapolation of measurements in boreholes C and D.

In order to trigger infiltration from the surface of the slope and thus represent the average effect of rainfall on steady-state flow in the model, two different approaches can be adopted. In the first approach, a low pore pressure, in the order of 0.1–0.2 kPa, is applied on the ground surface, alternatively, in the second one an appropriate constant amount of inflow is applied. For instance, these boundary conditions have been utilized in the rock mass flow models by Zangerl et al. (2003) and Cappa et al. (2004), respectively. Clearly, in DEM models, the aforementioned conditions must be applied to the single joints intercepting the upper boundary of the slope.

For the analysis of Chiascio slope it was preferred to impose the boundary inflow. Besides, it was decided to consider the inflow

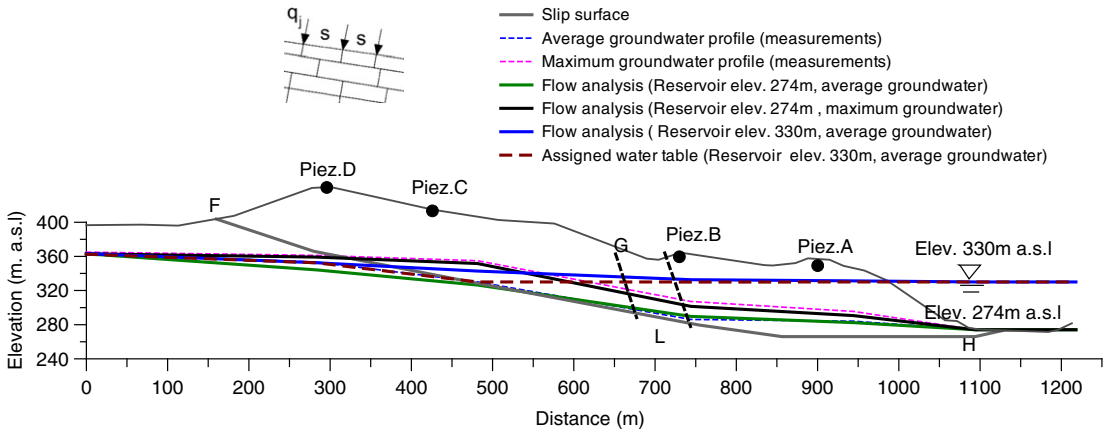

Fig. 26. Average and maximum elevation of the groundwater profiles (interpolated boundary of the water saturated joints) calculated by the flow analysis for empty reservoir (water level at 274 m a.s.l.) and completely filled reservoir (water level at 330 m a.s.l.): the dotted lines represent the observed profiles while the solid lines are model results.

magnitude as a model variable to be calibrated with the goal of satisfactorily matching the average measured or expected distribution of groundwater pressure in the slope. Of course, the inflow amount to each joint should not cause overpressures which can lead to mechanical failure (i.e. slip or opening of near surface joints).

Two different calibrations of the inflow have been performed to match, respectively, the average (AGW) and the maximum (MGW) measured groundwater pressure distribution (Fig. 26). In the first case, the final calibrated inflow is 0.1×10^{-5} m^3/s for the joints located between the piezometer D and the left boundary of the model, while a relatively higher inflow of 0.2×10^{-5} m^3/s is required for the joints from D to the toe of the slope. The MGW conditions can be reasonably matched by increasing only the latter inflow to 2×10^{-5} m^3/s.

The strategy herein adopted for the calibration of the hydro-mechanical model deserves a more general discussion. Two main points of the procedure must be stressed: i) the hydro-mechanical parameters of the single joint are realistic, i.e., preserve their effective physical meaning; ii) the calibration process affects only the inflows, which are regarded as instrumental variables to obtain the best fitting of piezometer data. On the contrary, it is impossible to preserve the real amount of overall discharge in the slope, because only a few joints are represented in the DEM model: the joint network is necessarily idealized and the joint spacing is much higher than the real one. As a consequence, it is neither meaningful to compare the overall inflow in the model with any estimate of effective infiltration, e.g., from the hydrological balance of the slope.

One of the curves in Fig. 27b represents the response of the slope to the progressive reduction in friction along the basal slip surface when the reservoir is empty (water elevation al 274 m a.s.l.) and the groundwater flow is calibrated for the AGW conditions. In this case, the displacement vs mobilized friction curve is similar to the curve obtained by the "water table" approach (compare Figs. 25c and 27b): the critical friction angles are almost the same although the displacements are slightly higher.

Also summarized in Fig. 27 is the predicted response of the slope to the progressive filling of the dam reservoir. The rising of the water level has been subdivided in steps, initially of 5 m and then of 10 m. For each reservoir elevation, a new hydro-mechanical analysis has been performed, changing only the water pressure boundary condition at the toe of the slope, with the inflow in the upper joints kept constant. The basal friction is also kept constant ($\varphi = 9°$) and the coupled flow-mechanical calculation is stopped when steady-state flow conditions are reached. Then, the calculation mode is switched to mechanical equilibrium only, with water pressures frozen. Therefore, this stage of the analysis is uncoupled and the strength reduction process is applied, for each reservoir elevation, without any change in water pressure during the SRM process.

Fig. 27a shows the predicted "displacement rate" (measured in millimeter/meter) of the control points N3 and N8 for $\varphi = 9°$. This "rate", already utilized in Fig. 25b, is given the displacement increment divided by the increase in water level. For reservoir levels up to 300 m a.s.l., the displacement increments predicted by the coupled analysis are very low and comparable to the approximated solution, but for higher levels the response is different. The displacement increments are significantly larger than those calculated by the uncoupled analysis, also plotted in the figure.

The influence of reservoir level on slope stability is more regular: the response curves obtained by the SRM for different water levels are almost homothetic (Fig. 27b), but the limit threshold (critical friction angle of the slope) is progressively shifted to the right. The difference in mobilized friction angle between the two cases of "empty" and "full" reservoir is slightly less than 1°, which can be regarded as a small reduction in stability but yet significant if compared to the low residual friction of the clay gouge.

A tentative "physical" explanation of the model response may be interesting, particularly for the phase of reservoir filling. Note that the displacement increment during infilling must be related to the change in water pressure distribution with respect to the initial situation of empty reservoir, characterized by higher pressure gradient in horizontal direction, particularly in the upper part of the slope. Change in buoyancy and seepage forces have counteracting effects during infilling. In fact, the upraise of water table (and buoyancy) reduces the normal effective stress on the slip surface, thus reducing the shear strength, but the decrease in horizontal seepage gradient also reduces the shear loads. The resultant effect depends on many geometrical and mechanical parameters and therefore is not easily predictable (not intuitive).

Furthermore, DEM models are characterized by localized and anisotropic flow conditions, as really occurs in jointed rock masses, particularly where the joint sets are few, as in the upper portion of the Chiascio slope. The groundwater profiles traced from the results of flow analysis (Fig. 26) are only average curves interpolating the isolated points (joints) where the water pressures are defined. Therefore, the comparison with "water table" or continuum flow models can be more effectively performed in terms of resultant effects (e.g., displacements, mobilized strength).

The engineering implications of these numerical modellings are twofold. The assessment of failure limits of the slope, for different hydraulic conditions and by different approaches, can be considered consistent, while the prediction of pre-failure behavior seems more problematic. The deformation response is significantly influenced by features of the slope model which can be only partially fixed and, therefore, need to be verified during the experimental stages of reservoir infilling.

7. Conclusions

The analysis of displacement measurements has shown that the Chiascio slope movement is characterized by an almost stationary velocity with seasonal accelerations due to the water pressure fluctuations, as high as ±10 m head during the 25 years of geotechnical monitoring. The time-lag between pressure increases in piezometers and rainfall was also analyzed. Peaks in piezometer levels seem best correlated with the 3-month cumulated rainfall.

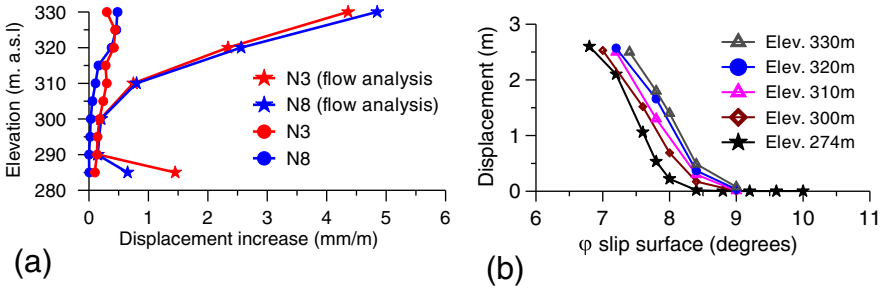

Fig. 27. Horizontal displacement increase calculated for the progressive filling of the reservoir by hydro-mechanical analysis, assuming $\varphi = 9°$ for the slip surface (b) (for comparison, the results of the uncoupled analyses with assigned water table are also plotted); curves of horizontal displacement (N3) vs mobilized friction angle for different reservoir levels.

The kinematics of the movement can be outlined as a compound mechanism in which a system of rock blocks is sliding on a low-inclination armchair-shaped surface. The shearing deformation is mostly localized in a thin band of tectonized clay gouge. Depth and lateral boundary of the movement can be clearly established only at the toe of the slope, on the base of inclinometer and geodetic target measurements.

The influence of different possible geometries of the slip surface on the critical friction angle has been investigated by DEM models, applying the Strength Reduction Method (SRM). The numerical models confirm the predominant role of a low-inclination sheared interbed within the Marly-Arenaceous formation. In any case, it was found that the limit strength of the slip surface is close to the residual friction of the clay gouge ($\varphi_r = 7.7°$).

Different reasonable hypotheses about the blocky structure of the slope (joint pattern, disarrangement) have been compared, finding a limited influence on the critical strength. Yet, the deformation mode of the slope is somewhat different if persistent or staggered joints are considered. The model with staggered joints exhibits less shearing along the inclined joint sets and more flexural bending around the knee-point of the slip surface.

The response of the slope to the change in water pressure in the joint network has been investigated by two different approaches: a simplified analysis, in which the pressure distribution is directly assigned by a "water table", or a coupled hydro-mechanical analysis, in which steady–state flow conditions are calculated, taking the interdependence of joint transmissivity and deformation into account. The results of the two analyses are significantly different. The displacement increment during the reservoir filling predicted by the coupled analysis are significantly larger, particularly for reservoir level higher than 300 m a.s.l.

The stability of the slope seems less sensitive to the increase in water level of the reservoir at the slope toe than to the rise of the groundwater table inside the slope. The difference in critical friction angle of the slope between the two limit situations of "empty" and "full" reservoir is slightly less than 1°, which can be regarded as a small reduction in safety conditions but yet significant if compared to the low residual friction of clay gouge.

From the modelling results, some relevant engineering implications can be derived: i) the failure conditions of the slope can be considered well defined: the basic mechanisms have been recognized, the results obtained for different hydraulic conditions and by different approaches are consistent; ii) concerns about safety issues are mostly related to the actual degree of strength mobilization of the clay interbed and its variability along the slip surface; iii) the simulation of the ongoing deformation of the slope is satisfactory, more problematic is the prediction of deformations caused by possible changes in groundwater conditions and water level at the slope toe; iv) the pre-failure displacements are significantly influenced by specific features of the hydro-mechanical model which can be defined only approximately and, therefore, need to be verified during the experimental stages of reservoir infilling, as already planned; v) similar uncertainties affect the design for slope stabilization and risk mitigation.

A specific merit of DEM models, compared to continuum models, is the realistic modelling of internal deformation and anisotropic flow in the sliding mass. Both these features have proven useful in the analysis of the Chiascio slope movement, but it is worthwhile to convey also some difficulties faced in DEM modelling, and the proposed solving strategies.

A first remark concerns the application of the SRM. In some case, it was relatively easy to identify a critical threshold in the "displacement vs mobilized friction" curve, i.e., a friction angle corresponding to a sharp increase in displacement, leading to plastic collapse. In other cases, particularly for DEM models with a complex blocky structure (e.g., many joint sets, staggered joints), it was found that the response curve may not exhibit an abrupt increment, but a progressively increasing gradient up to very large displacements. Therefore, it can be necessary to consider also a second characteristic value for the friction angle, corresponding to the threshold of "large displacements" (assumed equal to 3 m for the Chiascio slope), and particularly useful to compare the model response in different conditions.

A second remark is about the calibration of DEM models for coupled hydro-mechanical analyses. Considering that the joint spacing is much larger than real and the joint pattern is necessarily idealized, it seems difficult to use hydrological data (e.g., rainfall, effective infiltration). In the calibration strategy applied for the Chiascio slope, the real hydro-mechanical parameters of the single joint are fully preserved. The calibration process affects only the joint inflow from the ground surface, which can be regarded as an instrumental variable to obtain the best fitting of available piezometer data.

Acknowledgments

Special thanks to Prof. S. Olivero and Engineer S. Cola of EAUT for sharing their data and invaluable experience. The authors are grateful for the useful suggestions and comments of the anonymous reviewers.

References

Alonso, E., Pinyol, N.M., 2014. Slope stability in slightly fissured claystones and marls. Landslides http://dx.doi.org/10.1007/s10346-014-0526-5.
Alonso, E., Gens, A., Lloret, A., 1993. The landslide of Cortes de Pallas, Spain; a case study. Gèotechnique 43, 507–521.
Alonso, E.E., Pinyol, N.M., 2010. Criteria for rapid sliding I. A review of Vajont case. Eng. Geol. 114 (3–4), 198–210.
Angelucci, A., De rosa, E., Fierro, G., Gnaccolini, M., La monica, G.B., Martinis, B., Parea, G.C., Pescatore, T., Rizzini, A., Wezel, F.C., 1967. Sedimentological characteristics of some italian turbidites. Geol. Romana VI, 345–420.
Assefa, S., Graziani, A., Lembo-Fazio, A., 2014. Analisi di uno scivolamento planare in una formazione marnoso-arenacea. Incontro Annuale dei Ricercatori di Geotecnica -IARG Chieti e Pescara (in italian).
Assefa, S., Graziani, A., Lembo-Fazio, A., 2015. A deep seated movement in a marly-arenaceous formation: analysis of slope deformation and pore pressure influence. IOP Conf. Series: Earth and Environmental Science. 26. http://dx.doi.org/10.1088/1755-1315/26/1/012052.
Baldovin, G., 1968. La resistenza a taglio delle rocce con alternanza di strati litologicamente eterogenei. Rivista Italiana Geotecnica. 4, pp. 170–181 (in italian).
Barton, N., 2002. Some new Q-value correlations to assist in site characterization and tunnel design. Int. J. Rock Mech. Min. Sci. 39, 185–216.
Boon, C.W., Houlsby, G.T., Utili, S., 2014. New insights into the 1963 Vajont slide using 2D and 3D distinct-element method analyses. Gèotechnique 64, 800–816.
Brideau, M.A., Stead, D., 2012. Evaluating kinematic controls on planar translational slope failure mechanisms using three-dimensional distinct element modelling. Geotech. Geol. Eng. 30, 991–1011.
Cai, M., Kaiser, P.K., Uno, H., Tasaka, Y., Minami, M., 2004. Estimation of rock mass deformation modulus and strength of jointed hard rock masses using the GSI system. Int. J. Rock Mech. Min. Sci. 41, 3–19.
Cappa, F., Guglielmi, Y., Soukatchoff, V.M., Mudry, J., Bertrand, C., Charmoille, A., 2004. Hydromechanical modeling of a large moving rock slope inferred from slope levelling coupled to spring long-term hydrochemical monitoring: example of the La Clapière landslide (Southern Alps, France). J. Hydrol. 291, 67–90.
Celluzzi, E., Graziani, A., Lembo-Fazio, A., 2014. Analysis of a deep-seated slope movement in a marly-arenaceous formation. Int. Conf. Eurock Vigo paper 643, 1–6.
Dawson, E.M., Roth, W.H., Drescher, A., 1999. Slope stability analysis by strength reduction. Gèotechnique 49 (6), 835–840.
D'Elia, B., Picarelli, L., Leroueil, S., Vaunat, J., 1998. Geotechnical characterisation of slope movements in structurally complex clay soils and stiff jointed clays. Rivista Italiana Geotecnica 3, 5–47.
Grana, V., Tommasi, P., 2013. A deep-seated slow movement controlled by structural setting in marly formations of Central Italy. Landslides http://dx.doi.org/10.1007/s10346-013-0384-6.
Graziani, A., Rossini, C., Rotonda, T., 2012. Characterization and DEM modelling of shear zones at a large dam foundation. Int. J. Geosci. 6, 648–664.
Graziani, A., Rotonda, T., Tommasi, P., 2009. Stability and deformation mode of a rock slide along interbeds reactivated by rainfall. 1st Italian Workshop on Landslides. Napoli 1, 62–71.
Hammah, R.E., Yacoub, T., Curran, J.H., 2009. Variation of failure mechanisms of slopes in jointed rock masses with changing scale. In: Diederichs, M.S., Grasselli, G. (Eds.), Third Canada-U.S. Rock Mechanics Symposium (Toronto, Canada, Paper 3956).
Hatzor, Y.H., Levin, M., 1997. The shear strength of clay-filled bedding planes in limestones back analysis of a slope failure on a phosphate mine, Israel. Geotech. Geol. Eng 15, 263–282.
Hoek, E., Diederichs, M.S., 2005. Empirical estimation of rock mass modulus. Int. J. Rock Mech. Min. Sci. http://dx.doi.org/10.1016/j.ijrmms.2005.06.005.

Itasca, 2011. UDEC-Universal Distinct Element Code Version 5 User's Manual. Itasca Consulting Group Inc, Minneapolis.
Kulatilake, P.H.S.W., Shu, B., 2015. Prediction of rock mass deformations in three dimensions for a part of an open pit mine and comparison with field deformation monitoring data. Geotech. Geol. Eng. 33, 1551–1568.
Kveldsvik, V., Kaynia, A.M., Nadim, F., Bhasin, R., Nilsen, B., Einstein, H.H., 2009. Dynamic distinct-element analysis of the 800 m high Åknes rock slope. Int. J. Rock Mech. Min. Sci. 46 (4), 686–698.
Lembo-Fazio, A., Tommasi, P., Ribacchi, R., 1990. Sheared bedding joints in rock engineering: two case histories in Italy. Proceedings on the International Symposium on Rock Joints (Leon, Norway. 83–90).
Oberti, G., Bavestrello, F., Rossi, P., Flamigni, F., 1986. Rock mechanics investigations, design and construction of the Ridracoli dam. Rock Mech. Rock. Eng. 19, 113–142.
Palmström, A., 2005. Measurements of and correlations between block size and rock quality designation (RQD). Tunn. Undergr. Space Technol. 20, 362–377.
Ribacchi, R., 1987. Rock mass deformability. Insitu tests, their interpretation and typical results in Italy 2nd international symposium Kobe. Field Measurements in Geomechanics 1, 171–192.
Stavropoulou, M., 2014. Discontinuity frequency and block volume distribution in rock masses. Int. J. Rock Mech. Min. Sci. 65, 62–74.
Tommasi, P., Verrucci, L., Campedel, P., Veronese, L., Pettinelli, E., Ribacchi, R., 2009. Buckling of high natural slopes: the case of Lavini di Marco (Trento-Italy). Eng. Geol. 109, 93–108.
Witherspoon, P.A., Wang, J.S.Y., Iwai, K., Gale, J.E., 1980. Validity of cubic law for fluid flow in deformable rock fracture. Water Resour. Res. 16 (6), 1016–1024.
Yerro, A., Pinyol, N.M., Alonso, E.E., 2015. Internal progressive failure in deep-seated landslides. Rock Mech. Rock. Eng. http://dx.doi.org/10.1007/s00603-015-0888-6.
Zangerl, C., Eberhardt, E., Loew, S., 2003. Ground settlements above tunnels in fractured crystalline rock numerical analysis of coupled hydromechanical mechanisms. Hydrogeol. J. 11, 162–173.
Zhang, L., Einstein, H.H., 2004. Using RQD to estimate the deformation modulus of rock masses. Int. J. Rock Mech. Min. Sci. 41, 337–341.